Comparison between Experimental and Theoretical Results using Cuntze's 'Failure Mode Concept' model for Composites under Triaxial Loadings
- Part B of the WWFE-II -

R. G. Cuntze

D-85229 Markt Indersdorf, Germany. Tel.: 0049 8136 7754, Ralf Cuntze@t-online.de
formerly MAN Technologie AG, Augsburg, Germany

Summary

The Second World-Wide Failure Exercise (WWFE-II) deals with the behaviour of isotropic and unidirectional (UD) material as well as of multi-directional laminates composed of UD laminas subjected to a tri-axial state of stress. This paper represents a contribution using Cuntze's Failure Theory which is composed of four parts: (1) The Failure Mode Concept (FMC), to model the failure behaviour by UD Failure Conditions that assess tri-axial states of stress, (2)The establishment of non-linear stress-strain modelling of the embedded UD lamina material (in strain-hardening and strain-softening regime); and (3) The generation of a suitable computer code for carrying out non-linear analyses of multi-directional laminates under 3D stresses. In addition to WWFE-I is to consider part (4) Modelling of the matrix behaviour in ultra-high hydrostatic pressure domains.
The application of the FMC to a UD lamina results in five failure conditions. These take into account the material-symmetry of the UD lamina homogenized to a 'material'. Again, the UD lamina is treated as a transversely-isotropic material which is consistent with the WWFE-I.

Part B focuses on correlating the predictions with the experimental results provided. These involve 12 test cases, wherefrom the 7 UD cases are directly applicable for the validation of strength failure conditions (parts 1, 2). The analysis considers non-linearity of material and of geometry in case of changes of the fibre orientation angle. Special emphasis has been put on the difference between an isolated (weakest link) and an embedded lamina (in-situ behaviour) which possesses redundancy within the laminate.

After regarding lack, scatter and partial inconsistence of the provided test data in some test cases, the correlations look promising. However, a full 3D-judging of the UD failure conditions is not yet possible. At least, one can conclude: Generally it is physically not accurate to predict a failure surface with the knowledge of strength data, only! Bottlenecks were the parts 3 and 4.

Keywords: UD-lamina failure conditions, tri-axial stressing, hydrostatic compression, multidirectional laminates, non-linear behaviour

Nomenclature

Unidirectional lamina notions

a_s, b_s: Ramberg-Osgood parameters in softening regime

$b_{\perp\perp}$, $b_{\perp\parallel}$: Curve parameters due to friction in the UD lamina (solid material)

$E_1 = E_{//}$, $E_2 = E_3 = E_{\perp}$: Elastic moduli of a UD lamina in the directions x_1, x_2, x_3

Eff: Resultant stress effort of all interacting failure modes (corresponds to Puck's exposure factor f_E) which 'quantifies the risk of failure'. Failure occurs when this value becomes 1 or 100%

Eff^{mode}: Material stressing effort of a UD lamina in a failure mode, e.g. $\sigma_{eq}^{\parallel\tau} / R_{\parallel}^c = Eff^{\parallel\tau}$

E_{1f}: Elastic modulus of filament

$e_{\parallel}^t, e_{\parallel}^c$: Tensile and compressive failure strain of a UD lamina in x_1 direction

$F^{\parallel\sigma}, F^{\parallel\tau}, F^{\perp\sigma}, F^{\perp\tau}, F^{\perp\parallel}$: Failure functions for the 2 FF and 3 IFF

G_{21}, G_{21sec}: In-plane shear modulus of a UD-lamina; secant shear modulus

I_{23-5}: Combined invariant of the transversely-isotropic UD lamina

m : Mode interaction exponent

p_{hyd}: Hydrostatic pressure (positive value, whereas σ_{hyd} is sign-dependent)

p_1, p_2, p_3 : pressure values at the respective cross-section surfaces

$R_{p0.2}$: Stress value at 0.2 % permanent plastic tensile strain ($R_{c0.2}$ for compression)

$\hat{R}_z$: thickness crushing strength (better resistance) of the structure laminate

$R_\parallel^t \equiv X^t, R_\parallel^c \equiv X^c$: UD tensile and compressive (basic) strength parallel to the fibre direction

$R_\perp^t \equiv Y^t, R_\perp^c \equiv Y^c$: UD tensile and compressive strength transverse to the fibre direction

$R_{\perp\parallel} \equiv S$: Shear strength of a UD lamina transverse/parallel to the fibre direction

$[T_\varepsilon]$: Transformation matrix for strains

V_f : Fibre volume fraction

x_1, x_2, x_3: Coordinate system of a UD lamina (x_1 = fibre direction, x_2 = direction transverse to the fibre, x_3 = thickness direction)

x, y, z: Coordinate system of the laminate

α : fibre orientation angle with positive direction from x to $x_\parallel \equiv x_1$

ε_1, ε_2, ε_3: Normal strains of a UD lamina

$\gamma_{12} = \gamma_{21}$; $\gamma_{13} = \gamma_{31}$; $\gamma_{23} = \gamma_{32}$: associated shear strains of a UD lamina

v_{12}: Major Poisson's ratio in WWFEs (corresponds to $v_{\perp\parallel}$ in German VDI guideline. Tsai calls in his latest book the major Poisson's ratio - back again - v_{21}, as with the VDI guideline!)

$\mu_{\perp\parallel}, \mu_{\perp\perp}$: UD material friction values

σ_1, σ_2, σ_3: Normal stresses of the stress vector $\{\sigma\}$ of a UD lamina

σ_2^c; σ_1^t : In-plane compressive stress across; tensile stress in fibre direction

$\sigma_{\parallel}$, $\sigma_\perp$: Stresses parallel and transverse to the fibre direction

σ_z : Through-thickness compressive stress at the surface of the compressed laminate

$\hat{\sigma}_z^{cr}$: Through-thickness compressive fracture stress (= average crushing strength) of laminate

$\breve{\sigma}_1$: Filament fracture regarding equivalent stress ($\breve{\sigma}_1 = \sigma_f \bullet V_f \cong \varepsilon_\parallel \cdot E_f \bullet V_f = \varepsilon_\parallel \cdot E_\parallel$)

σ_{eq}^{mode} : Equivalent stresses of a mode ($\sigma_{eq}^{\parallel\sigma}, \sigma_{eq}^{\parallel\tau}, \sigma_{eq}^{\perp\sigma}, \sigma_{eq}^{\perp\tau}, \sigma_{eq}^{\perp\parallel}$) including load-induced mechanical stresses and residual stresses. An equivalent stress σ_{eq} is always positive such as the associated strength which was defined a positive quantity

$\hat{\sigma}$, $\hat{\varepsilon}$: Average laminate stress, strain (smeared over thickness)

σ_{1f} : Stress in filament

$\tau_{12} = \tau_{21}$, $\tau_{13} = \tau_{31}$, $\tau_{23} = \tau_{32}$: Associated shear stresses of a unidirectional lamina due to elastic symmetry. The first subscript locates the direction normal to the plane at which the shear stress is acting; the second subscript indicates the direction of the shear force

$\tau_{\perp\parallel}$, $\tau_{\perp\perp}$: Shear stressing transverse/parallel and transverse/transverse to the fibre direction

Abbreviations
CLT : Classical Laminate Theory
F   : Failure function

FF : Fibre Failure
FMC: Failure Mode Concept
FRP : Fibre-Reinforced Plastic
IFF : Inter-Fibre Failure
NF : Normal Fracture (fracture type)
SF : Shear Fracture (fracture type)
Tr : Tri-axiality factor, isotropic: $\sigma_{mean}/\sigma_{eq}^{Mises} = (I_1/3)/\sqrt{3 \cdot J_2}$
TrF : Trigger factor to consider mutual damage triggering of doubly acting IFFs (total
     common damage is higher than the sum of damages of the acting single failure modes)
w.r.t. : with respect to.

Indices, signs

c, t   : compression, tension (German Guideline VDI 2014)
ef   : effective
f, m   _: fibre, matrix
fr   : fracture
n   : repetitions in stack, Ramberg-Osgood exponent, number of performed tests
res   _: resultant
s   _: symmetric lay-up, softening
'   : denotes the lamina stresses in the x, y, z-system
-           : strength average (a statistically-based strength design allowable in design verification
              as well as the general strength are indicated with no bar over R)
+, x   : test points (squares indicate a UD strength)
σ, τ : indicate the failure induced by the normal Mohr stress or the shear Mohr stress
$1 \, kbar \equiv 100 MPa = 100 N/mm^2$.

1 Introduction

  Tri-axial failure states are often encountered: in submarines, bolted and screwed joints, bearings such as sealed polymer bearing cartridges pressurized up to 600 MPa, in cases of impact and ballistics, and other applications like high pressure vessels, anchor points of tension cables in civil engineering, load carrying UD hangers of helicopter blades, load introduction points, CFRP tubes for deepwater umbilicals, underwater blast. In consequence, there is a strong need to validate failure conditions in the multi-axial compression domain.

  The author has made a contribution to WWFE-II, Part A, in order to determine the capability of current theories for predicting failure in composite laminates under tri-axial stresses, see [Cun10]. The present paper is one of a series of papers related to the WWFE-II, Part B, where the author and originator of the Failure Mode Concept (FMC) compares the theoretical predictions for 12 different Test Cases (TC) with the provided twelve sets of associated experimental data. The model involves the following: (a) proposing appropriate nonlinear stress-strain curves for the UD lamina before and after occurrence of initial failure, (b) taking into account the effect of pressure on mechanical properties, and (c) incorporating the 5 failure modes (2 Fibre-Failure (FF) and 3 Inter-Fibre-Failure (IFF), see *Figs. 1* and *2),* into a suitable quasi-global form.

  Proving the capability of the tri-axial FMC theory requires realistic, well evaluated, and well understood experimental data. Therefore, this paper at first describes and investigates the

experimental data and secondly comments on the experiments before finally comparing them with the predictions. And this, after correction of mistakes, that have nothing to do with the FMC and after an estimation of non-provided friction parameter values on basis of the Part B information.

2 Cuntze's Failure Mode Concept-based Failure Theory

2.1 General

A full failure analysis is understood here to be composed of the previously mentioned four parts: (1) Failure conditions to assess multi-axial states of stress (see *Fig. 1*), (2) Non-linear stress-strain curves of the UD lamina material as input (see Part A), (3) Non-linear coding for obtaining a realistic response of the laminate, and (4) the 'hydrostatic pressure' matrix model. Cuntze's method of applying his FMC methodology to brittle UD material is to propose a set of five failure conditions describing the five pure failure modes in a lamina and then interact these conditions by a suitable probabilistics-based 'series spring model'. The number five is mandatory according to the material symmetry of the transversely-isotropic UD material (modelled as an *ideal* crystal). A lamina is seen here to be macroscopic, as used in the past.

In the usually faced loading situations - according to the inherent brittle behaviour of the UD material - failure means fracture failure and yielding failure does practically not exist. Only, the constituent matrix experiences some yielding (most often used matrices exhibit $\varepsilon^{fr} \geq 6\%$). At the most, a so-called quasi-yielding from diffuse damaging or micro-cracking at the stress concentration locations within the lamina will occur. Then, in the failure process follow first filament breaks and a growing of localized micro-cracks that initiate micro-delamination. All this might be termed 'quasi-yielding' before real delamination takes place.

Key features of the FMC, published in WWFE-II, Part A, are listed in *Table 1*. Some aspects shall be recalled or added here:

* Driven from the shortcomings of the usual *'global fitting'* strength conditions the originator Cuntze looked for a *'failure mode-related fitting'* on basis *of material symmetry* and for the use of *invariants, related to physical mechanisms*.

* Sufficient for pre-dimensioning is the knowledge of the basic strengths. A remaining unknown curve parameter *b* in the author's *modal* failure conditions concerns the friction μ of the UD material (the *real* crystal experiences friction). It's value can be approximately estimated. The more brittle the material behaves the larger μ will be. Friction parameters are physically required. Not physically-based *global* failure conditions do not use such a parameter and this leads to a shortfall.

* Whether a fracture type is termed NF or SF depends on the addressed model level: For IFF3 in *Fig. 2* holds that the fracture type may be a NF (constituent micro-level) or a SF (lamina macro-level).

2.2 Assumptions for modelling in the WWFE-II

- Pore-free material, specimen surfaces polished and well sealed
- Fibre volume content is constant ($V_f = 60\%$), tube specimens have no warping
- Perfect bonding of the layers is assumed here, no layer waviness, edge effects do not exist

- Performance of the micro-mechanical analysis, needed for the consideration of the so-called 2^{nd}Tg effect had to be executed with own micro-mechanical formulas (had to be adjusted) since the mandatory formulas have been not provided. As micro-mechanical data are fully linked to the formula set they have been determined with, it is a shortfall, when micro-mechanical data are provided without the associated formulas.
- Part 4: The onset point of the decrease of the slope with modulus and shear strength of the matrix is allocated to a kink at $p_{hyd} = 200 MPa$ and modelled linear beyond.
- Analysis necessarily sticks to the transversely-isotropic UD lamina material. This is in line with WWFE-I, the more, as specific thickness properties could be sparsely provided.

2.3 Conclusions from previous investigations

- The FMC has proven to be a helpful tool in simply fitting the course of multi-axial material strength test data. Its excellent mapping of in-plane multi-axial strengths has been proven in the WWFE-I, sometimes first, after being capable to re-evaluate the originally provided test data due to finally provided additional information as for instance for TC 2 and TC 7 in WWFE-I, Part B.
- It is an effective concept that utilizes a *strict* failure mode thinking as well as the application of *material symmetry-related invariants* which are dedicated to a volume change or a shape change or to the material's internal friction the homogenized material element may experience
- It can capture all UD failure modes in one equation but avoiding a shortcoming of the usual 'global fitting' strength conditions
- The friction curve parameter b in the friction-related failure conditions IFF2 and IFF3 can be transferred into a Mohr-Coulomb-related condition and thereby physically assessed. Then, it can be related to a material friction value μ that can be measured according to the Part A Annex.

Notes for 2D and 3D applications of UD failure conditions:

1.) $\sigma_2 \cong \sigma_3$: Activates the failure mode IFF1 in 'two planes' and thereby 'doubles' fracture danger

2.) τ_{23}: Activates two different failure modes, i.e. IFF1 and IFF2, according to the fact that the shear stress τ_{23} can be replaced by a normal tensile stress σ_2^t with a compressive stress σ_2^c. This fact causes a problem for the automatic insertion of stresses into the IFF2 material stressing effort. It was practically considered in the MathCad program by employing principal stresses in the quasi-isotropic 2-3 domain, putting two queries ($\sigma_I = 0$, if $\sigma_I \geq 0$; and $\sigma_{II} = 0$, if $\sigma_{II} \geq 0$), and inserting the principal stresses into IFF2 instead of the lamina stresses $\sigma_2, \sigma_3, \tau_{23}$, see Annex 2.

3.) In progressive failure analysis, for the post-initial failure (softening domain beyond IFF), the assumption of a non-uniform decay of stiffness (and of effort) and not the assumption of a sudden death is of advantage for a stabile numerical computation. This further brings a benefit as it involves some sort of numerical damping, see figure 4 in Part A.

4.) In the development of the FMC-based failure conditions in Annex 1, formulated in material stressing efforts, just those stresses have been 'proportionally stressed' up to fracture failure which are mode failure driving (see Part A text).

5.) In the WWFE, the use of the term fracture stress in case of a multi-axial fracture stress state would be better than strength. Strength is a specific technical term for a uni-axial fracture stress in strength analysis (see Standards). Further, the term fracture stress or fracture state of stress describes the fact better. Fracture behaviour is sensitive to surface flaws, internal micro-cracks and

debonding (but kissing) areas under tension and compression. A superimposed p_{hyd} significantly affects this behaviour and is of benefit for the load-carrying capacity.

3 Details of possible refinements of the analysis and changes in modelling

3.1 FMC-based failure conditions and non-linear analysis

There is no reason for a modification of the UD failure conditions and the modelling of the strain-softening curve of the embedded lamina since WWFE-I-Part A was issued. Only, due to a change in matrix behaviour, provided in Part B by the organizers, matrix modelling had to be changed from ductile to semi-brittle behaviour.

Also the non-linear analysis was still executed by the simple secant-modulus procedure as described in Part A. As program, MathCad 13 was taken again.

3.2 Re-work of the matrix model in ultra-high compression domain

In the WWFE-II, as fourth part of the failure theory, the behaviour of the matrix under ultra high tri-axial pressure should be investigated. In Part A, the author could not sufficiently model this special behaviour. Ultra-high pressures are not subject of usual practical applications in the design of load-carrying structures. A deeper investigation of the provided test results was necessary and lead to an improved 2^{nd}Tg effect modelling. Thereby, the full pressure effect was separated into an elasto-mechanical part (Birch, see Part A) and a material part (matrix weakening) that is addressed below.

Considering *elastic stiffness*, from the various cited references a coarse approach can be constructed on basis of gathered test results for the shear modulus, Refs. [Pae77; Pae96, fig.5],. This approach seems to be relatively generally valid for the epoxy matrix family. The kinked curve in *Fig. 3* can be fitted in the usual high pressure domain in a bi-linear manner by the function (series spring model applied again)

$$f_{2ndTg}: 1 \text{ if } p_{ef} < 200MPa \text{ , and } 1 - a_f \cdot (p_{ef} - 200MPa) \text{ otherwise} \tag{1}$$

$$\text{with } p_{ef}: 0 \text{ if } \sigma_{hyd,ef} > 0 \text{ , and } -\sigma_{hyd,ef} \text{ if } \sigma_{hyd,ef} < 0$$

with a_f as fitting parameter, representing the decay of the slope in *Fig. 3,* and the reduction factor f_{2ndTg}. The effect on the moduli at room conditions can be tackled by

$$G_m = G_{m0} \cdot f(2^{nd}Tg) \quad \text{with} \quad G_{m0} = E_{m0}/(2 + 2 \cdot v_{m0}). \tag{2}$$

To be inserted into this equation is the effective hydrostatic stress $\sigma_{hyd,ef}$ in the constrained matrix material point at the envisaged critical location within the embedded constrained lamina. The decay of the slope of stiffness and 'strength' in the ultra-high hydrostatic domain was tackled in Part A by a blind preliminary approach which used the mean stress in the matrix material as effective hydrostatic stress $\sigma_{hyd,ef} = I_1/3 = -p_{hyd,ef}$. This had to be refined in order to tackle the usually different normal stresses. Hence, the approach was changed in Part B to the Eqs.(3) as improved engineering approach to capture the 2^{nd}Tg-effect

$$\sigma_{ef,m} = \max(\sigma_{1,m}, \sigma_2, \sigma_3). \tag{3a}$$

In the case of tri-axial and lateral bi-axial compression (σ_2, σ_3) of a lamina the state of stress $\sigma_{1,m}$ in the fibre-constrained matrix has to be used. It is generated because the stiff fibres

prevent a free matrix elongation and build up an effective hydrostatic compression stress in the matrix. Micro-mechanical equilibrium leads to the relationship

$$\sigma_{1,m} = -\sigma_f \cdot V_f /(1-V_f) = -\varepsilon_1 \cdot E_{\parallel} \cdot V_f^2 /(1-V_f) \tag{3b}$$

employing $\sigma_f = \varepsilon_1 \cdot E_{\parallel} \cdot V_f$. The mathematically highest stress is effective. Both quantities, $\sigma_{ef,m}$ and $\sigma_{1,m}$ are sign-dependent. This means, pressure is inserted as a negative value and a hydrostatic tensile stress as a positive value. Unfortunately, the author could not validate the Eqs.(3) by the provided test information.

For the matrix strength, Pae showed in [Pae96] that the decay of the slope is higher than that for the moduli. Due to a lack of sufficient information, the decay of the slope or the reduction of the moduli decrease, respectively, would be also applied to multi-axial strength.

Note that modelling of the 2ndTg effect has nothing to do with the applicability and quality of the FMC-based failure conditions.

3.3 Transfer to UD stiffnesses and UD strengths

For the UD material, the 2ndTg-effect will differ from that which is obtained for the pure matrix, the effect is usually minor. However in the Test Cases, lacking of knowledge for the UD materials, the strength reduction factor f_{2ndTg} might be simply transferred from the matrix to the multi-axial UD fracture stresses.

3.4 'Strength' decrease and 'healing'

According to the usual failure condition $\sigma_{eq}(\{\sigma\})/\overline{R} = 1$ the load-carrying capacity increases with a 'lower' σ_{eq}-value and with a higher strength $\overline{R}$. Therefore, the positive multi-axial pressure-based lowering of the equivalent stress σ_{eq} should be not mixed up with an increase of the material property, the strength $\overline{R}$. The effect of pressure with respect to a 'healing' of the 'diffuse' micro-cracking situation is inherent in the lamina and the laminate high pressure test data (e.g. TC 2). It needs to be separately modelled, whenever applicable.

3.5 Consideration of in-situ effect of the embedded lamina

Properties used as input for the analysis are test results from *isolated* UD lamina specimens such as a tensile coupon. They are load-controlled derived and results of weakest link type whereas the in-situ behaviour of an *embedded* UD lamina is deformation-controlled and therefore of redundant type. This fact shows up that a good mapping of the course of 'isolated UD test data' does not involve the full information necessary for a qualified analysis of laminates which consist of a stack of embedded laminas.

4 Brief descriptions of Test Cases and comments on Part B test data provided

4.1 Description of test specimens

In this paper an attempt is made to validate a *theoretical model of the reality* by *some experimental realisations of the reality.* To accomplish this, 12 challenging Test Cases are provided by the WWFE-II organisers [Kad09] involving (see table 4 in Part A):
  (a) Epoxy material under a tri-axial state of stress

(b) 0° unidirectional lamina under various tri-axial states of stress

(c) [0/90]$_s$, [±45/90/0]$_s$, [±35]$_s$ multi-directional laminates under various tri-axial states of stress and through-thickness loadings, and

(d) three stress strain curves for
- 0° unidirectional laminas under various tri-axial states of stress
- [±35]$_s$ laminates under a tri-axial state of stress and
- [0/90]$_s$ laminates under through-thickness compression.

It is to be noted for the TC test specimen shapes: TC1 is a full matrix cylinder, the used TC 2,3,4,8,9 results are based on thick-walled hoop wound tubes, TC5 is a rectangular block, the TCs 6,7 (from Parry, Wronski) are dog-bone shaped machined from pultruded rods, the TCs 10,11 are waisted (dog-bone shaped) tubes milled from a laminate block, and the TC12 a waisted solid laminate specimen. The not-used 0°-TC2, TC3 tubes are not wound but hot-press moulded tubes. Above variations in test specimens (manufacture etc.) have a different effect on the quality of the envisaged validation. In total, 9 different tri-axial (non-)failure domain envelopes and 3 stress strain curves have to be correlated. The following section comments the provided experimental data input.

4.2 Comments on experimental input

Stresses and strengths: A UD lamina consists of the constituents fibre, matrix and interphase ($\neq$ interface). The interphase is usually considered by the IFF related material property. After homogenization, the UD lamina is called UD material. For the UD material element, *Fig. 1* depicts the 3D state of stress $\{\sigma\} = (\sigma_1, \sigma_2, \sigma_3, \tau_{23}, \tau_{31}, \tau_{21})^T$. In the coming text for varying quantities such as stresses the subscripts 1, 2, 3 are utilized, and sometimes in figures - for clarity - the dedicated symbolic signs for stresses.

Because of the symmetries of the transversely-isotropic UD material, modelled an ideal crystal, there are 5 basic strengths and 5 elasticity properties, only. Therefore, the characterisation of strength requires the measurement of 5 independent basic lamina strengths (in brackets the US denotation): $R_\parallel^t (= X^t)$ and $R_\parallel^c (= X^c)$ as tensile and compression strength parallel to the fibres; $R_\perp^t (= Y^t)$ and $R_\perp^c (= Y^c)$ as tensile strength and compressive strength transversal to the fibre direction); and $R_{\perp\parallel} (= S)$ as in-plane shear strength. The 5 strengths are given in the old symbolic denotation, used again in the German guideline VDI 2014, in order to avoid misunderstanding in the application of material properties as FEA input. It is standard to measure above five strengths, which read, incorporated in a vector, $\{R\} = (R_\parallel^t, R_\parallel^c, R_\perp^t, R_\perp^c, R_{\perp\parallel})^T$. Usual convention is: Positive direction of lamina orientation angle is from x to fibre direction x_1, fibre in hoop direction of a tube is 90° to the axial direction.

Making an attempt to understand the provided experimental results one has to distinguish whether the test results are fracture values in total stresses or hydrostatic pressure superposed fracture stresses. This difference is not always clearly written in the given test information. From comparing data of various sources one can only sort out what might be meant. Due to *Fig. 4*, for the example UD lamina, tri-axial failure information can be provided in several ways ($\sigma_{hyd} = -p_{hyd}$) using a stress σ that is often termed differential stress:

$$\{\sigma\} = (\sigma_1, \sigma_2, \sigma_3, \tau_{23}, \tau_{31}, \tau_{21})^T \qquad \text{or}$$

$$\{\sigma\} = (\sigma_1{}^{add} - p_1, \sigma_2{}^{add} - p_2, \sigma_3{}^{add} - p_3, \tau_{23}, \tau_{31}, \tau_{21})^T \qquad \text{or} \qquad \text{(4a,b,c)}$$

$$\{\sigma\} = (\sigma_1{}^{add} - p_{hyd}, \sigma_2{}^{add} - p_{hyd}, \sigma_3{}^{add} - p_{hyd}, \tau_{23}, \tau_{31}, \tau_{21})^T$$

with a p_i, as absolute pressure value, acting at a cross-section surface. The stresses σ^{add} are the 'external' stresses which may be increased up to σ_{fr}^{add}. This is the resistance value that marks the pressure-dependent multi-axial fracture state of stress. In order to correctly interpret the diagrams in the associated literature one has to carefully check whether the diagram is of the type $\sigma_{x,fr}(\sigma_y = \sigma_z, \overline{R})$ or of $\sigma_{x,fr}(p_{hyd}, \overline{R})$. *Fig. 4* proves that the data are identical.

In order to interpret and use the test data (not all are clear) correctly it is of basic interest to understand what is behind, what are test specimen and test rig (examples TC 10, 11). In this context, TC tests, test specimens, and test data are commented in detail in the next chapters beginning with some "information phrases" typical for the TC.

4.3 Discussion of Test Data and Associated Information provided for Part B

TC1 : $\sigma_{x,fr}(\sigma_y = \sigma_z)$, matrix MY750epoxy

"Test data from a sealed cylindrical bar epoxy specimen in a container filled with a highly pressurized fluid [Hin05]. The axial loading is carried out by a pull rod. The necessary two seals cause friction which is considered in the provided fracture stress data. The axial fracture stress is computed from the measured load divided by the original cross-section".

Barrelling was not monitored!
Not all physically needed properties, such as the (low) material friction of this *semi-brittle* matrix material, could be provided by the organizers.
- Also, modelling the matrix behaviour beyond the epoxide-typical -200*MPa* (*equal* compressive stresses) slope, kinking point was not supported. This, the more meets the difficult 2ndTg-matrix modelling under 3D compression loading with *different* stresses in the three coordinate directions. Information for modelling the change of stiffness and 'strength' is not directly given, and in literature the data vary. Therefore a correction factor f_{2ndTg} has to be assumed for stiffness and for 'strength' as well. If TC-applicable, both, for stiffness and 'strength' the same value is taken, namely an assumed 10% decay of the slope between -200 *MPa* and, arbitrarily, -600*MPa*.
Unfortunately, literature could not fill the lack of information. Instead, a discrepancy was found: Beyond the kinking point, Youngs modulus E still increases in [Hin05] with a distinct (lower) slope whereas in [Shin-Pae92, Pae95] the related shear modulus G_m is decreasing. Of course, there is no strong relationship between E and G anymore ($E \neq G \cdot (2 + 2 \cdot \nu)$), but also Birch's formulas (Part A) do not confirm such a different behaviour.
- In [Hin05] is reported: *All test specimens under compression failed by yielding* (for Part B the failure type yielding was corrected by the reviewer into fracture which is essential). This holds from atmospheric pressure up to $p_{hyd} = 400MPa$. The failure description in the compression domain will be modelled by a low *b* friction parameter value of $b_\tau^c = 0.18$. Note that $b_\tau^c(\mu = 0) = 0$ means 'Mises yield cylinder' and full yielding.

- The provided data set forms a straight line and thereby does not show any 2^{nd}Tg-effect, Fig.TC1a. On the contrary, beyond the indicated kink level (at about $-200 MPa$) the Fig.TC1c shows a widening of the failure surface instead of a shrinking. It looks as if the effect needs not to be addressed for this matrix material. However, for a visualisation of the tendency of the $2^{nd}Tg$ shift effect a 10% slope decay is assumed and displayed in the Figs.TC1a, TC1c.

<u>Note</u>: In Fig.TC1c so-called Lode coordinates $I_1/(\sqrt{3}\cdot\overline{R}_c)$ and $\sqrt{2\cdot J_2}/\overline{R}_c$ are applied. They possess the same scale in the full stress space.

Modifications from Part A to Part B: As the providers have changed the information on the matrix behaviour from yielding to fracture the friction model parameter $b(\mu)$ had to be increased for Part B. No change of the FMC model itself must be made.

TC2 : $\tau_{21}^{fr}(\sigma_2=-p_{hyd})$, UD T300-PR319epoxy (as for TC3, TC4)

The test results obtained from the two test specimen types show wide scatter and jumping. Test data does not show a 2^{nd}Tg-effect. Investigated are only the 90° tubes. An investigation, why the data set of the twisting 0° tube is not used (see **Fig. 5**), is performed in *Annex 5*.

- The tubes are relatively thick-walled. This means for torsion, that the *shear stress* grows from inner to outer radius. Therefore, τ_{out} is failure-responsible. The shear strength increases from the inner to the outer radius according to the following formula (see [Shi92]) $\tau = 2\cdot M_T\cdot r/[\pi\cdot r_{out}^4\cdot(1-r_{inn}^4/r_{out}^4)]$, and $\tau_{out}\cong 1.4\cdot\tau_{inn}$. It is assumed that τ_{out} is the provided shear stress. For information, the application of the shear stress formula for the thin-walled tube delivers a $\tau_{thin}=0.88\cdot\tau_{out}$ which is a smeared value. So, the outer wall surface is the critical location.

For the other critical stress, the filament *hoop stress* and its strain $\varepsilon_f\equiv\varepsilon_\parallel$, the critical cylindrical location has to be sorted out, whether it lies at the inner radius or at the outer radius. Due to the elastic behaviour in radial direction, the hoop stress σ_1 changes from a positive value at the inner radius to an outside negative compressive value. However, not σ_1 is responsible for fracture but σ_{1f}. This means, σ_1 has to be replaced by $\breve{\sigma}_1\cong\varepsilon_\parallel\cdot E_\parallel$ to simply achieve that.

- A FEA check delivered a filament hoop strain at about $\varepsilon_{fr}^{\parallel t}=-0.74\%$ and an extreme stress gradient. This means that shear fracture IFF3 may be overtaken at the $p_{hyd}=600 MPa$ level (large scatter underwalls this) by a relative sudden occurring FF2. Also, structural collapse may occur. Closing of the failure surface will be the result of the common actions of material failure FF2 and structural failure of the tube.

Theoretically from simple elastomechanics, the hydrostatically loaded tube will break at $p_{hyd}=R_{//}^c/(1-2\cdot\nu_{\perp//})=950/(1-2\cdot 0.32)=2600 MPa$. This is a guess if the tube remains structurally stabile and if $\nu_{\perp//}$ remains constant. A consideration of the unknown 2^{nd}Tg effect will terminate the curve earlier.

- Novel idea: At a first look, the jump in data size at $\sigma_2=0$ or at shear strength $R_{\perp//}$ is not clear because it is the same shear failure mode IFF3. An explanation for the jump is the 'healing' or the redundantly acting hydrostatic pressure effect. In order to fit the course of

data on an average the shear strength is increased up to a model value of $107 MPa$ regarding redundancy. The non-provided friction curve parameter $b_{\perp//}$ in the shear function below

$$\tau_{21} = \sqrt{-b_{\perp//} \cdot \sigma_2 \cdot R_{\perp//} + R_{\perp//} \cdot \sqrt{(b_{\perp//} \cdot \sigma_2)^2 + R_{\perp//}^2}}$$ is the result of an optimal mapping of the

course of test data including the check point (inverse parameter identification).

Finally, a rounding 'down' to $\overline{R}_{\perp\|} = 97 MPa$ (isolated value) can be performed by using a correction function $f_{TC2} = (1 - c_3 / e^{-\sigma_2 / c4})$ with $c_3 = 0.093$, $c_4 = 22$ that leads from the 'isolated' strength point to the course of 'embedded' test data.

- For TC2 and TC3 an average stress-strain curve must be used. This curve could not be well assessed by the Part A data and because the friction parameter $b_{\perp//}$ was not provided.

- The thick wall has an effect for tubes with high hoop stiffness such as the 90° tubes and marginal effect in case of 0° tubes.

- The 90° reinforced tubes have the bottleneck of a rapidly altering hoop stress over the radius under radial pressure and the 0° tubes experience under torsion a turning of fibre orientation. Due to the turning of the fibre direction under torsion the 0° tubes experience a much more complicated and different stress state than the 90° tubes and can therefore not put together in the same diagram, see *Annex 5*.

- For the 90°-test specimen the torsion moment causes a τ_{21} shear stress. Note that, this stress is the failure shear stress and not the associated τ_{12}.

Modifications from Part A to Part B: TC2 and TC3 have to use an average (typical) stress-strain curve. This could be first obtained from Part B knowledge. Having known the average curve in Part A, the predicted curves would not differ from the Part B ones.

TC3 : $\gamma_{21}{}^{fr}(\sigma_2 = -p_{hyd})$

"In the case of 90° tubes the shear strength and the strain to fracture increase approximately by 43% and 65%, respectively, from atmospheric pressure up to $p_{hyd} = 600 MPa$, [Hin10]. Failure was reported to have taken place by matrix shear or interfacial debonding. The fracture surface contains various major intrinsic defects such as interlaminar cleavages or locally delaminated areas, and cracks, and it also shows some clean debonded traces and exposed fibres, and resin debris. At 600MPa, the fracture surface was non-uniform, with less defects, and shows that plastically deformed resin residues adhering to fibres".

The required TC3 curve is a fitting curve through all the fracture points of the shear strain-shear stress Ramberg-Osgood curves (R-O was the chosen fitting function, all its four R-O parameters vary with p_{hyd} or σ_2, respectively) according to the formula in TC4

$$\gamma_{fr,\sigma2} = \tau_{fr,\sigma2} / G_{\sigma2} + 0.002 \cdot (\tau_{fr,\sigma2} / R_{\perp\|, 0.2, \sigma2})^{n_{\sigma2}}. \tag{5}$$

- The jump in data size at $p_{hyd} = 0$ can be explained again by the 'healing' (redundancy) influence of the hydrostatic pressure effect. In order to map the course of data on an average the fracture shear strain at atmospheric pressure is increased up to $e_{\perp\|} = 10.4\%$. The provided course of test data permits to simply fit the test data (thin line) by a linear (Pae proved, curve must be almost straight) approach, between the 'check point' and the above failure strain $e_{\perp//}$,

$$\gamma_{fr}(\sigma_2) = c_1 + c_2 \cdot \sigma_2 \quad \text{with} \quad c_1 = 0.104, \ c_2 = -6.33 \cdot 10^{-5}. \tag{6}$$

- The final rounding procedure is performed analogously to TC2 by a correction function

$$f_{TC3} = (1 - c_3 / e^{-\sigma_2 / c4}), \quad \text{with} \quad c_3 = 0.173, \ c_4 = 22. \tag{7}$$

Modifications from Part A to Part B: In Part A the fitting approach was solely based on results from Shin and Pae, and the author's estimation of fracture values.

TC4 : $\tau_{21}(\gamma_{21})$ *under* $p_{hyd} = 600MPa$

"Test data from [Shi92a, Shi92b]. Thick hollow circular cylinders as 90°-tube test specimens. At minimum, 3 tests were carried out at each condition of pressure. Shear was introduced by application of a torque to the end of the test specimen".

According to the obtained experimental data the investigation of the TC2 through TC4 begins with the mapping of provided shear stress-shear strain data. The generated curve will be a single curve ($\equiv$ one test realisation) within the scatter band of the provided curves. For the envisaged strain-hardening FRP materials this curve will be engineering-like mapped by

$$\varepsilon = \sigma / E_0^{mode} + 0.002(\sigma / \overline{R}_{p0.2}^{mode})^n \tag{8}$$

because the well-known MIL-Handbook 5 applies it as an engineering mapping tool, that is recognized in industry for this type of material behaviour. The R-O exponent

$$n = \ell n\left(\varepsilon_{pl}(R_m)\right) / \ell n\left(\overline{R}_m^{mode} / \overline{R}_{p0.2}^{mode}\right) \tag{9}$$

is estimated from a strength point $\left(\overline{R}_m^{mode}, \ \varepsilon_{pl}(\overline{R}_m^{mode})\right)$ and a yield or, here, more as a quasi-yield point information. The description of the stress-strain curve requires 4 R-O parameters, where the 'strength' value $\overline{R}_m(p_{hyd})$ is just one of them. Mapping needs the use of average properties. From the Part A information a guess of this value could be obtained. Yield 'strength' $\overline{R}_{c0.2}(p_{hyd})$ and the physically necessary $b_{\perp\parallel} = 0.12$ had to be estimated.

- The degree of the strain-hardening non-linearity mainly affects $E_\perp^c$ and $G_{//\perp}$. It depends on the non-linearly behaving matrix material, the '2ndTg-shift effect', and the *finite strain*-related 'Birch effect'. The effect of 2ndTg would have caused that the fracture stress *increase* under p_{hyd} is *reduced* and fracture shear strain is increased.

- Novel idea: There must be a link between TC2, TC3 (both the curves result from a bunch of different test specimen curves) and TC4 (single curve of the bunch). This link, marked by a common check point (hollow square) in the three figures, can be only obtained if the TC4 single curve is replaced by an average (typical) shear stress-shear strain curve.

For performing this, it is assumed that the centre of the 'fracture stress/fracture strain domain' is the most probable, 'average' failure point. The idea above to obtain an average curve is effortful, because all R-O parameters of each curve change, and no similarity can be stressed:

1.) Basic average 'isolated' curve, for orientation: $\gamma_{21} = \tau_{21} / G_{\parallel\perp} + 0.002 \cdot (\tau_{21} / \overline{R}_{p0.2,\perp\parallel})^n$,

   constructed from provided UD data set and information from [Pae96]

   $n = 6.9$, $\overline{R}_{\perp\parallel,0.2} = 74MPa$, $\overline{R}_{\perp\parallel} = 97MPa$, $\gamma_{\perp\parallel,fr} = 0.086$, $G_{\parallel\perp} = 1330MPa$.

2.) Prediction of average $\gamma_{21} = \tau_{21} / G_{\perp//}^{600} + 0.002(\tau_{21} / \overline{\tau}_{21,0.2}^{600,pred})^{n^{600}}$ on available data

04.04.2014

- Estimation of a shear fracture value at $p_{hyd} = 600 MPa$ using the IFF3 equation:

$$Eff^{\perp//} = \{[\, b_{\perp//} \cdot I_{23-5} + (\sqrt{b_{\perp//}{}^2 \cdot I_{23-5}{}^2 + 4 \cdot \bar{R}_{\perp//}{}^2 \cdot (0 + \bar{\tau}_{21,fr}^{600,pred\,2})^2}\,] / (2 \cdot \bar{R}_{\perp//}{}^3)\}^{0.5} = 1$$

with $I_{23-5} = 2 \cdot \sigma_2 \cdot (\tau_{21,fr}^{600,pred})^2 + 0 + 0$, $\sigma_2 = -p_{hyd} = -600 MPa$, $b_{\perp//} = 0.3$

obtaining $\bar{\tau}_{21,fr}^{600,pred}(b_{\perp//} = 0.3) = 193 MPa$ in Part A, instead of $137 MPa$ for $b_{\perp//} = 0.12$.

- Determination of remaining properties to compute the R-O parameters, estimated by using information from Pae-Shi curves ([Pae96]): $G_{\perp//}^{600} \approx 1.13 \cdot G_{\perp//} = 1503 MPa$, $\gamma_{\perp//,fr}^{600} = 0.152$, and the remaining needed R-O parameters could be estimated as $n^{600} = 5.5$ and $\bar{\tau}_{21,0.2}^{600,pred} = 125 MPa$

- Above data based on $b_{\perp//} = 0.12$ would practically lead to the Part B curve.

3.) Provided test data, *single* curve: $\gamma_{21} = \tau_{21} / G_{\perp\parallel}^{600} + 0.002 \cdot (\tau_{21} / \tau_{21,0.2}^{600})^n$,

$n = 3.8$, $\tau_{21,0.2}^{600} = 125 MPa$, $\tau_{21,fr}^{600} = 161 MPa$, $\gamma_{\perp\parallel,fr}^{600} = 0.154$, $G_{\perp\parallel}^{600} = 1503 MPa$

4.) Searched Part B *average* (bar over) curve: $\gamma_{21} = \tau_{21} / G_{\perp\parallel}^{600,av} + 0.002 \cdot (\tau_{21} / \bar{\tau}_{\perp\parallel,0.2}^{600,av})^n$,

$n = 4.6$, $\bar{\tau}_{\perp\parallel,0.2}^{600,av} = 70 MPa$, $\bar{\tau}_{\perp\parallel}^{600,av} = 140 MPa$, $\gamma_{\perp\parallel,fr}^{600,av} = 0.142$, $G_{\perp\parallel}^{600,av} = 1503 MPa$.

Modifications from Part A to Part B: Change from estimated $b_{\perp//} = 0.3$ to 0.13 (Part B). Therefore, Part A showed a pretty blind prediction.

TC5 : $\sigma_2^{fr}(\sigma_3 = \sigma_1)$, UD E-glass/MY750epoxy,

"Test data from [Hin05], compression tests: rectangular blocks (5 x 5 x 20 mm³ coupons, cut from filament wound UD panels) under combined axial loading with lateral pressure. During test, the (hydrostatic) pressure was first increased to a pre-determined level and then kept constant while σ_2^c was increased continuously until the specimen fractured".

Task is the prediction of the failure envelope in all quadrants. Test data are provided for tri-axial compression in quadrant III, lower branch, only. They look good but do not indicate any 2ndTg effect by a kink point or deflection point, respectively. A comparison can be only made in quadrant III.
- The slope of the course of test data shows that the UD material is less brittle than assumed in Part A. Therefore, the friction parameter $b_{\perp\perp} = 1.21$, estimated in Part A, was lowered to 1.16. As lateral strength, the Part A value $\bar{R}_\perp^c = 145 MPa$ is to be kept (organizers) despite of the fact that in case of mapping an average value of the three Part B-provided compressive test data of 132 *MPa* should have been taken. This has an effect on well mapping the test data.

Modifications from Part A to Part B: Change $b_{\perp\perp} = 1.21 \rightarrow 1.16$, $b_{\perp\parallel} \equiv \mu_{\perp\parallel} = 0.3 \rightarrow 0.2$. Part A curve would coincide with Part B if friction parameters could have been provided for Part A.

TC6 : $\sigma_{1,fr}(\sigma_3 = \sigma_2)$, UD S-glass/epoxy

"Test data set for the forth quadrant is from Zinoviev, and for the third quadrant from Wronski-Parry [Wro82]. Wronski-Parry used dogbone test specimens cut from pultruded rods. Tests were carried out under pressures p_{hyd} up to 300 MPa. Failure was reported to be catastrophic where kink band was formed (FF2) *at approximately 30 degree relative to the fibre axis, up to 300 MPa. Increasing the pressure led to an increase of the compressive 'strength' of the material. The nonlinear behaviour under shear and transverse compression was similar to that observed in the E-glass UD response. Wronski and Parry measured a compressive strength of $\overline{R}_{\parallel}^c = 1150 MPa$. The rest of the provided values were assumed"*.

The test data of TC6 and TC7 show large differences in quadrant IV. For mapping of the tension curve FF1 in quadrant IV no reliable test data set was provided. TC 6 presents a diffuse scatter in quadrant IV. This can be explained from own tests with NOL (Naval Ordinance Laboratory) rings. It is known that the additional bending stress at tensioning the NOL ring causes pretty a stochastic fracture with a fracture level pretty lower than that from the usual coupon test. A stadium ring would have delivered better results but is more difficult to produce. Therefore, the results from Zinoviev cannot be used for validation.
- The tendency of the left branch, mode FF2, from *Wronski-Parry* (quadrant III) is the same as in TC7, fortunately, and could be a validation basis. The left branch indicates a kink and thereby – for the first time possibly – seems to indicate some 2[nd]Tg effect.
- In TC3 and TC4 was demonstrated that the shear fracture strain increases with p_{hyd}. This will also occur in the case of tensile fracture strain due to the beneficially acting (healing) of p_{hyd}. However, it is to be sorted out which portion belongs to the Poisson effect (governed by $\nu_{\perp\parallel}$) and which portion to a healing effect. The author predicted the almost linear increase of the compressive fracture stress with p_{hyd} in a test case cited in [Rhe95] by employing just the Poisson effect, that always causes tensile pre-straining. Incomprehensible, this was not successful in case of TC6 and TC7.
- TC7 is the better test case for deeper investigations than TC6 and shall be discussed. Just the fibre material is different, glass changes to carbon.

Modifications from Part A to Part B: None.

TC7 : $\sigma_{1,fr}(\sigma_3 = \sigma_2)$, UD A-S/epoxy

"Test data from Parry-Wronski [Par82, Par85]. Tests executed with dog-bone test specimens, as before. Failure modes observed are longitudinal splitting, kinking, kink band".

The course of the test data indicates that the predictions in Part A may have been performed on basis of a not really understood 2[nd]Tg-matrix modelling. However, still now, some discrepancies disturb the use of the provided test data for model validation.
Due to missing test points the provided thickness strength $\overline{R}_z = 38 MPa$ will be not used. It will be sticked to the UD model and not moved to an orthotropic model.
- Test data look better than in TC6. However, it is not understood why the tendency of the curves in quadrant III and IV is so different. Primarily, Poisson is acting at smaller bi-axial states of compression stresses first, the 2[nd]Tg effect comes later. Therefore, due to the Poisson effect the compressive fracture failure strain and similar the failure stress in quadrant III,

which acts at the cross section, is increased and in quadrant IV the tensile failure strain (right curve) is reduced. This would result in a similar curvature tendency.

With increasing failure strain the compression curve becomes more horizontally and the tension curve more vertically. How long the vertical drop will go (the provided data set ends at $\sigma_2 = \sigma_3 = -300 MPa$) is not demonstrated. In contrast note, that it is proven in [Hine05] , that the tensile fracture stress will reduce with p_{hyd} till $-860 MPa$ and this is in the sense of an acting Poisson effect.

- In quadrant IV, it looks at $-150 MPa$ either as if the fracture strain is reduced or as if the Poisson effect would have doubled. Below the bi-axial compression level of $\sigma_2 = \sigma_3 = -300 MPa$, the Poisson effect 'vanishes' and the tensile stress, acting at the cross-section, keeps the same value of about $1500 MPa$. In other words, the fracture strain of the filament would increase. Usually, the matrix reduces stiffness and this would increase the Poisson effect and cause the opposite curvature or tendency of the provided data curve. It would become flatter instead of steeper or even vertical. Also, if the interphase between filament and matrix breaks then the bi-axial pressure will cause an elongation of the filament linked to its Poisson's ratio ν_f which is not so much different to the UD value ν_{12} .

- All the courses of the provided test data and of other test data have a flattening tendency as it is also depicted in quadrant III. From this might be questioned whether measurement or evaluation of the provided test data might be not adequately performed, at least in quadrant IV. Influence on the curves have the in-plane major Poisson's ratio ν_{12} (the smaller ν_{12} is, the steeper the curve), the 'healing' effect from bi-axial compression (may increase failure strain), and the 2ndTg effect. The author is not able to physically explain the discrepancies.

Modifications from Part A to Part B: None

TC8 : $\sigma_{y,fr}(\sigma_z = \sigma_x)$, E-glass/MY750epoxy, laminate [35/-35/35/-35]$_{ns}$

"Test data from [Kad10b]. Test specimens were filament wound tubes (water-hose, convention: 55° winding angle w.r.t. axial direction or 35° to the laminate axis) *without any coating. In the tests, an equal internal and external lateral pressure, surrounding the test specimens, was first increased up to a pre-determined value; then an axial compression load was incrementally applied, while the pressure was maintained constant during the test, till fracture failure took place. Failure is indicated by a drop in the axial load. The hoop, axial and radial stresses were computed from the three dimensional behaviour of thick tubes using orthotropic thick cylinder theory as described in [Kad98]. It should also be noted that the axial stress could be approximated using the following calculation:*

$$\sigma_z = (F - p_{hyd} \cdot \pi \cdot d^2)/A + p_{hyd} \qquad (10)$$

with A being the cross section area of the tube and d the diameter of the piston rod. The total axial stress (σ_z) is that due to net axial compression load F, acting over the cross section of the specimen, and that due to end pressure p$_{hyd}$, acting over the thickness".

  Data for the upper branch is missing. Data for the quadrants I, II, IV could be not provided in order to have a 'round' foundation for the validation. The high values of the 3 test data at the positive $\hat{\sigma}_y$-axis will have to be explained. *Fig. 6* describes test arrangement and stresses.

- A re-investigation of the friction parameter $b_{\perp\perp} = 1.21$ showed that it had to be reduced to 1.16 as for TC5. This value is substantiated by information from WWFE-I. The other friction parameter $b_{\perp\parallel} \equiv \mu_{\perp\parallel}$ is obtained by mapping the test data provided in quadrant III. Note, that TC5, TC8 and TC9 possess the same material (see table 2 in Part A) but are different test specimens that will naturally cause some difference in 'strengths'.

- An improved non-linear programming is necessary, especially due to the fact that in TC9 both the failure modes IFF2 and IFF3 have a similar risk to fracture, or - in other words - the material stressing effort is similar for both modes in the envisaged two-fold failure domain.

- The fibre volume contents for Part B was increased from the initial *60%* up to $V_f = 67\%$ ("dry" filaments possible) This would make a correction necessary so that the TC8 data do not remain the same as for TC5, but, the driving strengths in the *compression* domain $\bar{R}_{\parallel}^{c}, \bar{R}_{\perp}^{c}. \bar{R}_{\perp\parallel}$ might not become better. Therefore the values for $\bar{R}_{\parallel}^{c}, \bar{R}_{\perp}^{c}$ are kept.

An increase of the fibre volume content on the elasticity properties is not considered due to the other uncertainties and that the stress-strain curve would have to be adapted and hardening parameters to be reworked with all its work consequences.

Modifications from Part A to Part B: Change of $b_{\perp\perp} = 1.21 \rightarrow 1.16$, $b_{\perp\parallel} \equiv \mu_{\perp\parallel} = 0.3 \rightarrow 0.2$. *With the Part B knowledge the same curve would have been obtained in Part A.*

TC9 : $\sigma_{y,fr}(\sigma_x = \sigma_z = -100MPa)$, *properties. see TC8*

"Test data from Kaddour et al. Test specimens, see TC8. Pressure surrounding the specimen was first incrementally increased up to approximately -100MPa, so that the specimen is essentially under the same pressure at the inside, outside and at the end. The specimen was then subjected to an axial compression load, while the pressure was maintained constant during the test. The results showed that the strains are negative under the action of hydrostatic pressure. As the axial tensile load (stress) is applied, the strain in the hoop direction started increasing and then became positive at around -150MPa of stress, while the strain in the loading direction increased in the negative (compressive) direction."

Data for ε_z are missing. The final state of stress does not show a 2[nd]Tg effect.

Modifications from Part A to Part B: Change of $b_{\perp\perp} = 1.21 \rightarrow 1.16$, $b_{\perp\parallel} \equiv \mu_{\perp\parallel} = 0.3 \rightarrow 0.2$.

TC10 : $\tau_{yz,fr}(\sigma_z = \sigma_x)$, IM7/8551-7, quasi-isotropic laminate [45/-45/90/0]$_{ns}$

"Test data from DeTeresa [Ter01, Ter04]. Test specimens (termed waisted) *were tubes, machined from thick panels into small 'dogbone pieces' having a hollow cylinder gauge section and square ends for applying torque. The specimens were subjected to combined axial compression and shear (torque). A constant axial compression load was applied first and then the specimen was twisted to failure under torque control. The fracture stress of this quasi-isotropic laminate is expected to be higher than* $780MPa$. *Because DeTeresa et al. did not provide data for pure through-thickness compressive strength Kaddour et al, [Kad10], tested various specimens made of quasi-isotropic carbon/epoxy laminates under uniaxial through-thickness compression. They used 3 specimen configurations: thick cylinders* (solid waisted), *cubes and* (short hollow) *waisted specimens. They found a strong dependency of the fracture stress on the shape of the test piece".*

Fig. 7a shows a 90°-lamina of the stack of the thick-walled tube milled from a laminate block For comparison, *Fig. 7* depicts the traditional wound or tape-layered tube; $r_{inn} = 7.95mm$, $t = 2.55mm$, $t_k = 0.25mm$. In TC10 and TC11 short hollow waisted test specimens are used. For such a specimen, termed 'cylindrical' in [Kad10], an average strength of $\hat{\sigma}_z^{cr} = -783MPa$ (5 tests) was measured. However for the quasi-isotropc (not cross-ply, as TC 12 is marked!) solid waisted specimen (5 tests) of TC12 $\hat{\bar{\sigma}}_z^{cr} = -1363MPa$ was obtained. From the difference can be learned that hollow specimens fracture much earlier due to structural instability failure triggered by the previous material failure. Therefore, for the quasi-isotropic TC10 tube (angle-ply) and the waisted cross-ply tube TC11 the average 'solid' crushing strength $\hat{\bar{\sigma}}_z^{cr} = -1363MPa$ must be reduced for the prediction of the curve in the high compressive domain. Hence the recommendation of the reviewer, to use $\hat{\bar{\sigma}}_z^{cr} = -1363MPa$ for TC10 and for 11, cannot be followed. For TC10, as through-thickness compressive fracture stress (crushing strength) $\hat{\bar{\sigma}}_z^{cr,TC10} = -1000MPa$ is used as compromise.

Test situation does not generate a uniform stress state in the critical locations and a small stress gradient. With respect to the non-uniform shear stress field at the cross-section plane it can be stated that the test specimen does not give much experimental evidence. The specimen encounters *multi-site* failure within each lamina and at the same time *multi-ply* failure in all laminas. This means that a multi-fold fracture danger is given in the stack. The specimen is not an adequate tool to validate strength failure conditions. In *Fig. 7* maximum filament and matrix failure locations are indicated. These locations are bound to the varying lamina fibre orientation and take different positions over the stack. It can be assumed that the most critical location and the associated failure mode is IFF or matrix failure. Then the associated critical interlaminar stress state can be estimated.

Three different sub-stack descriptions are found in the provided documents:[45/-45/90/0]ns, [90/45/-45/0] and [45/0/-45/90] (from theoretical reasons a stack with minimum angle change would be best because it leads to the smaller interlaminar stresses to achieve compatibility of the lamina deformations). However, this does not have an effect because the specimen is milled from a laminate brick.

- The tube is thick-walled which means that the outer shear stress will be fracture decisive. For TC 10 and TC11 a lamina-to-lamina volume FEA would be necessary for stress analysis. In [Kre07] a 'smeared' model is presented that substitutes the effortful volume model. This helps to get a solution for the specimen's deformation behaviour. Finally however, the actual stress state at the critical location is required for strength judgement.

The friction parameter is determined by curve data fitting.

- Before using the provided approximate quasi-isotropic laminate's through-thickness (crushing or squeezing) fracture stress value $\hat{\sigma}_z^{cr}$ of the (structure) laminate in the (material) strength failure condition it should be thought how far the type of fracture might remain material failure. For instance, if filaments of the stacked layers come to lie upon another, this leads to a failure which is not covered by a material strength failure condition anymore. It is clear that crushing of a laminate is the "end" of further operational use. The crushing stress value is the consequence of several effects: micro-cracking, FF1, filament-upon-filament, edge effects, and structural instability. This means: A material failure condition can only partly predict this mixed failure phenomenon.

Modifications from Part A to Part B: TC10 was not investigated in Part A. A test curve is the result of both the partners, of test specimen and of test rig. In Part A, the author assumed an ARCAN test rig, loaded by scissor forces F , whereas in Part B the De Teresa torque test rig is used. This caused a change in the prediction of failure location and of type and curve.

TC11 : $\tau_{yz,fr}(\sigma_z = \sigma_x)$, IM7/8551-7, cross-ply laminate $[0/90/0/90]_{ns}$

" Test data from De Teresa [Ter01, Ter04], test execution as for TC10".
The dogbone-shaped tube test specimen TC11 has less different layer angles than TC10. Therefore, the fracture curve should be longer and lie a little higher than curve TC10 due to the fact that a lower number of critical locations (just 0° and 90°) is encountered. This fracture stress capacity, higher than for TC10, is assumed to be $\hat{\bar{\sigma}}_z^{cr,\ TC11} = -1100 MPa$. Again, the solid block specimen of TC12 exhibits higher 'strength' than the TC11 tube.

Modifications from Part A to Part B: The test rig became known and the loading situation had to be fully reworked. The assumed crushing stress was increased from $\hat{\sigma}_z^{cr,TC11} = -780 MPa$ in Part A (used as minimum value of three points, safe side) up to $-1100 MPa$.

TC12 : $\hat{\varepsilon}_x(\sigma_z^c) = \hat{\varepsilon}_y(\sigma_z^z)$, $\varepsilon_z(\sigma_z^z)$; IM7/8551-7, $[0/90/0/90]_{ns}$

"No data was available from the work reported by DeTeresa et al. for this Test Case. Consequently, the organisers suggest experimental data that <u>could</u> be used a guidance illustrating the likely response of similar laminates (quasi-isotropic [45/0/-45/90]_{ns}) under through-thickness compression of solid waisted specimens, obtained by Kaddour et al. [to be published]".

It is not clear why this TC is marked as a cross-ply but the curve stems from a lay-up that is a quasi-isotropic angle-ply! The effect of the curing stress is of practical interest in the positive domain, and therefore not requested in quadrant III.
- The provided *similar* curve (provided in Part B) will be considered. It is one single curve of 5 experiments. The through thickness stress $\sigma_z^{max} = -1400 MPa \cong \hat{\bar{\sigma}}_z^{cr} = 1363 MPa$ (average of the 5 tests) is not marked as final fracture, however it may be from operational reasons assumed as the practical final fracture. In this context: The tube specimens in TC10 and TC11 finally show a structural failure, the TC12 waisted specimen not, but a full material crushing.
- The Part A curve does not have the tangent stiffness of the "similar" curve. Because a 3D-CLT delivered the same low initial slope it could be concluded that the transverse elasticity moduli $E_{\perp,in}$ of Part A and B do not correspond, and the provided elasticity modulus in thickness direction is too low and to be increased.
- A further effect is to be considered, namely, that with increasing thickness reduction the filaments are more and more pressed upon another and the composite modulus $E_{\perp z}$ approaches $E_{\perp f} = 19000 MPa$. To achieve this, the "similar" curve is to be mapped applying a simple quadratic approach ($\Delta\sigma_z = -1700 MPa$, $E_{\perp,in} = 11000 MPa$) through σ_z^{max} and origin

$$E_{\perp z}(E_{\perp f}) = E_{\perp,in} \cdot [(1 + \frac{E_{\perp f} - E_{\perp,in}}{E_{\perp,in}}) \cdot \frac{\sigma_z^2}{\Delta\sigma_z^2}] \ . \tag{11}$$

Modifications from Part A to Part B: Correction of a mistake (curvature of the predicted curve in Part A was opposite to the experimental curve caused by an error in the equations coded), and increase of initial lateral elasticity modulus at origin from $E_{\perp,in} = 8400 MPa$ (Part A) to $11000 MPa$ (Part B), and particularly, by consideration of a growing filament contact.

5 Comparison between theoretical predictions and experiments

Some additional figures are added to demonstrate special features of modelling and tests.

TC1 : Matrix MY 750, $\{\sigma\} = (\sigma_x,\ \sigma_y = \sigma_z,\ \sigma_z,\ 0,\ 0,\ 0)^T \equiv (\sigma_I, \sigma_{II}, \sigma_{III})^T$

Problem: How does tri-axial compression influence the failure behaviour if two components of the stress vector are equal?

Task: Determination of the tri-axial fracture failure curve $\sigma_{x,fr}(\sigma_y = \sigma_z)$, Fig. TC 1 and validation of the 2ndTg model of the matrix to capture Part 4, for the matrix at least.

It is well known from the cited literature and at QinetiQ that hydrostatic pressure stress states higher than 200*MPa* change the second glass temperature point of the matrix with the described stiffness worsening effect on the matrix. 2ndTg effect and Birch effect have been effortful implemented into the author's FMC-based 3D-CLT-MathCad program.

Comparison:

- Fig.TC1a: Mapping of provided test data in quadrant III with provided data (thin) and with an assumed *2ndTg* shift effect (bold) to show tendency in the case the assumed effect size would occur. The slope of the lower curve with the assumed 2ndTg-effect shows a reduction beyond -300*MPa*. This means that the compressive stresses $\sigma_y = \sigma_z$ have to be increased to carry the same load as without matrix weakening. A 10% slope decay starting at the kink point was considered between 200 and 600 *MPa*.

- Fig.TC1b: Predicted curves in the quadrants I, II, IV. An interaction of shear failure and normal failure in their transition zone in quadrant I by a simple linear approach in 3D space, characterized by Lode's coordinates, was not executed in Figs. TC1b and 1c, due to a lack of data in the transition zones.

- Fig.TC1c: Visualisation of provided test data in 3D space with provided data (dashed) and with an assumed *2ndTg* shift effect (bold).

- Mapping of test data, given in quadrant III only, could be achieved after describing shear failure in a more ductile way (Pat B information). This meant, lowering the unknown friction parameter from $b_\tau^c = 1.52$ (brittle) in Part A to 0.18. In this context one should recall that 0.18 almost reflects ductile behaviour and $b_\tau^c = 0$ means 'Mises yield cylinder'.

- A 2ndTg effect seems not to exist for the matrix . 2ndTg modelling – needed for the following TCs – could be not substantiated by the test data set provided.

- Course of given data could be well mapped. Interaction or out-smoothing in the transition zones SF-NF is not performed in Figs. TC1b and TC1c. Failure surface is not closed.

TC2 : UD lamina T300/PR319, $\{\sigma\} = (\sigma_1,\ \sigma_2,\ \sigma_3\ 0,\ 0,\ \tau_{21})^T$

Problem: Influence of hydrostatic pressure p_{hyd} on the in-plane fracture shear stress.

Task: Determination of the fracture failure curve $\tau_{21,fr}(p_{hyd})$ with $\sigma_1 = \sigma_2 = \sigma_3 = -p_{hyd}$, and p_{hyd} an absolute pressure value, Fig. TC2.

Comparison:

- Course of scattering 90° test data could be well mapped after considering the typical stress-strain curve and the hoop stress distribution (outer hoop stress is higher than the inner one).
- The sudden increase (jump) at zero hydrostatic pressure is assumed to be the consequence of the healing by p_{hyd} and was modelled by the simple approach mentioned. Then, the full course of the correlated test points could be mapped. 'Check point' for TC2 through TC4 is the open square in the three figures. It serves as verification of the approach.
- The failure curve is closed (still shown in Part A). To add to the Figures TC2 and TC3 a closed failure curve is speculative and adds no value to the comparison because the failure is no material failure anymore but very likely structural failure that cannot predicted by a strength failure condition.

TC3 : UD lamina T300/PR319, $\{\sigma\} = (-p_{hyd},\ \sigma_2 = -p_{hyd},\ -p_{hyd},\ 0,\ 0,\ \tau_{21})^T$

Problem: Influence of the hydrostatic pressure p_{hyd} on the in-plane fracture shear strain.

Task: Determination of the fracture failure curve $\gamma_{21}(\sigma_2^{fr}, \tau_{21}^{fr})$, Fig. TC3.

Comparison:

- Course of scattering 90° test data could be well mapped. The failure curve is closed.
- The sudden increase (jump) at zero hydrostatic pressure is assumed to be the consequence of the healing p_{hyd} and was modelled in the above simple way.

TC4 : UD lamina T300/PR319, $\{\sigma\} = (-p_{hyd},\ \sigma_2 = -p_{hyd},\ -p_{hyd},\ 0,\ 0,\ \tau_{21})^T$

Problem: Influence of an initially constant hydrostatic pressure on the in-plane shear stress-shear strain curve.

Task: Determination of the stress-strain curve $\tau_{21}(\gamma_{21}^{fr})$ for $p_{hyd} = 600\ MPa$. Hereby, the shear is superimposed on the still acting p_{hyd}.

Comparison:

- The determination of an average curve (bold) enabled to equally well map TC2 and TC3 and to show up the check point that links the curves.
- The provided single curve test data could be well mapped (dashed curve in TC4).
- The blind prediction of Part A, dotted curve, is included.

Note: The 'check point' ($\gamma_{21} = 0.142,\ \tau_{21} = 140 MPa,\ p_{hyd} = 600 MPa$) was intentionally not optimized, w.r.t. TC 2 and TC3 data mapping..

TC5 : UD lamina E-glass/MY750 Epoxy , $\{\sigma\} = (\sigma_1 = \sigma_3,\ \sigma_2,\ \sigma_3,\ 0,\ 0,\ 0)^T$

Problem, basically: How much lateral stress σ_2 can the UD material sustain if a fibre-parallel stress σ_1 acts which is equal to a through-thickness stress σ_3? Test practice: p_{hyd} is superimposed by a lateral compressive stress σ_2^c at the σ_2-surfaces.

σ_1 is the stress acting at the respective coupon surface; the diagonal is the $p_{hyd} - line$.

Task: Determination of the fracture failure curve $\sigma_{2,fr}(\sigma_1 = \sigma_3)$ in the quadrants III and IV.

Comparison:

- The course of provided test data could be well mapped. The failure curve is closed.
- Assuming that the model pre-requisites remain valid, final failure by kinking (FF2) is possible under p_{hyd} (see TC2 in section 4.3 and Part A, fig.TC5), according to the following relationship $E_{\parallel} \cdot \varepsilon_1 = -p_{hyd} \cdot (1 - 2 \cdot v_{12})$ with v_{12} as larger Poisson's ratio.

- Computation indicates wedge failure IFF2 in quadrant III. Under σ_3^t, IFF1 is final failure.

- For information: Test data from DeTeresa [DeTer99] for the upper branch (2nd solution) of the failure curve in quadrant III are lying on the predicted upper branch after being re-evaluated by subtracting p_{hyd}.

TC6 : UD lamina S-glass/Epoxy, $\{\sigma\} = (\sigma_1, \ \sigma_2, \ \sigma_3 = \sigma_2, \ 0, \ 0, \ 0)^T$

Problem: How much compressive fibre-parallel stress σ_1^c can the UD material sustain when a lateral compressive stress σ_2^c acts which is equal to a through-thickness stress σ_3^c?

Task: Determination of the tri-axial failure curve $\sigma_{1,fr}(\sigma_2 = \sigma_3)$.

Comparison:
- No mapping is possible in quadrant III, left branch or compressive branch. The provided strengths do not very fit to the provided data set (crosses)
- The tensile branch in quadrant IV cannot be used because the data have no experimental evidence for a validation.

TC7 : UD lamina A-S carbon/epoxy1, $\{\sigma\} = (\sigma_1, \ \sigma_2, \ \sigma_3 = \sigma_2, \ 0, \ 0, \ 0)^T$

Task: See TC 6, just the UD material of TC7 is different to TC6.

Comparison:
- No satisfactory mapping is possible in the quadrants III and IV. The course of data points exhibits probable contradictions that cannot be explained by the author (see section 4.3). Mapping is sufficient for $p_{hyd} < 150 MPa$, only.

Idea, concerning a probable error-prone data evaluation: The compressive curve would better match with TC7 data if the p_{hyd} value would have been subtracted from σ_1^c.

TC8 : Laminate E-glass/MY750 epoxide, $\{\hat{\sigma}\} = (\hat{\sigma}_x = \sigma_z, \ \hat{\sigma}_y, \sigma_z = -p, \ 0, \ 0, \ 0)^T$

Problem: Effect of the applied surface pressure $\sigma_z = -p$ (through-thickness stress) on the size of the normal section force n_y at fracture, when $n_x / t = \sigma_x$ and t is laminate thickness.

Task: Determination of the average laminate fracture stress $\hat{\sigma}_{y,fr}(\sigma_z = \hat{\sigma}_x)$. Curing stress from effective temperature $\Delta T = 120° \text{-} 23° = 97°$ is $\sigma_2^t = 15 MPa$.

Comparison:

The analysis follows in TC8 and TC9, as usually, the (non-FE) 3D-CLT-MathCad program.

- IFF1 at the positive σ_z axis belongs to the weakest link value or 'isolated' value $\overline{R}_{\perp}^t$, initial failure from σ_3^t means final failure. The curing stress has no direct effect, because it acts in the laminate plane.

- At the positive $\hat{\sigma}_y$ axis some redundancy governs and the *initial* failure behaviour is more benign. The curing stress has a direct effect. The provided 3 test data belong to *final* failure of this specimen at about $\hat{\sigma}_y^{final} = 72MPa$. This value can be explained: IFF1 micro-cracks decrease the stiffness and the fibre angle 35° increases. Under non-linear shear loading, more and more load is put onto the fibres until final failure occurs. Failure curve: closed.

- Mapping of test data is not fully satisfactorily in domains (valid for TC9, too) where the complicate non-linear treatment of the commonly acting two modes IFF2 and IFF3 (of about the same size of Eff^{mode}) is located. There, the MathCad program faced numerical problems for some stress combinations and did not converge correctly. With respect to the small data basis $b_{\perp\parallel}$ was kept 0.2 and not increased to 0.25 for optimum mapping. Birch considered.

TC9 : Laminate E-glass/MY750 epoxy , $\{\hat{\sigma}\} = (-100MPa,\ \hat{\sigma}_y,\ -100MPa,\ 0,\ 0,\ 0)^T$

Problem: Effect of the applied surface pressure $\hat{\sigma}_y = n_y / t$ on the in-plane average strains $\hat{\varepsilon}_x, \hat{\varepsilon}_y$ at fracture, when $\hat{\sigma}_x = \sigma_z = -100MPa$ remains constant from beginning.

Task: Determination of the stress-strain curves $\hat{\sigma}_{y,fr}(\hat{\varepsilon}_x, \hat{\varepsilon}_y, \hat{\varepsilon}_z)$. Curing stress: $\sigma_2^t = 15MPa$.

Comparison:

For low values p_{hyd} , no 2ndTg effect is to be considered, Birch effect is considered, however.

- Initiation of shear failure IFF3 triggers final wedge failure IFF2. This doubly non-linear task could not be handled sufficiently well.

- Mapping of test data is pretty good in the usual engineering domain, however not satisfactorily in the high strain domains because of the complicate treatment of the acting two-fold failure behaviour. For explanation: With Mises, just one failure mode is to be treated and not two as here.

Keep in mind: The usual design requires, due to functional and design requirements, strain values less than 0.5% = 0.005.

TC10 : Laminate IM7/8551-7, $\{\hat{\sigma}\} = (0,\ 0,\ \sigma_z,\ 0,\ 0,\ 0)^T$

Problem: Effect of an applied surface pressure $\sigma_z = -p$ ($\hat{\sigma}_x = \hat{\sigma}_y = 0$) on the angle-ply laminate's out-of-plane shear capacity. The pressure is imposed by a pressure head, the shear stress by a torque at the quadratic ends.

Task: Computation of the inter-laminar failure shear stress $\tau_{zy} \equiv \tau_{yz}(\sigma_z)$ of a non-rotational symmetric, short, and waisted tube test specimen (Fig.7a) which was milled from a thick laminate block. In contrast to a rotational wound or tape-layered tube with its intra-laminar shear stresses, the torque is now introduced via inter-laminar shear stresses τ_{31}, τ_{23}.

Curing stress from effective temperature $\Delta T = -177° + 23° = -154°$ is $\sigma_2^t = 22MPa$. This stress, however, acts intra-laminarly or in the laminate plane, respectively.

04.04.2014

Comparison:

Danger to failure, indicated by the material stressing effort, is encountered at multiple sites along the circumference of each single lamina and in addition − angle alternated - in all laminas at the same time.

The test specimen cannot be simply modelled, FEA is mandatory without having any simplifications from circumferential symmetry. Stress analysis would require a 3D material/geometrical nonlinear FEA. This means that the FMC would have to be implemented into a source deck which is too costly. After analysis, the FE stress results obtained for TC10, TC11 and TC12 would have to be transferred into stresses that are judgeable by strength conditions because the stack does not 'produce' a non-uniform stress distribution in the critical locations.

Therefore, stress state and distribution at the critical locations of TC10 and TC11 have been investigated and it was found that the sole consideration of the 3 interlaminar stresses $\sigma_3, \tau_{31}, \tau_{23}$ in the FMC conditions might be a good approach. A simple linear strength model was applied at the critical location which considers the acting inter-laminar stresses. A second aspect is the termination of the curve at the assumed laminate crushing. This is captured by adding a crushing effort $Eff^{cr} = \sigma_z / \hat{\sigma}_z^{cr}$ in Eq.(A4).

- Failure responsible in the compression domain are the shear stresses. Computation indicates shear failure IFF3 (is initial and final failure) before 'crushing' failure comes to act at $\hat{\sigma}_z^{cr}$.

- In order to well map the course of test data a pretty low interaction value (safe side) of $m = 2.5$ was taken in TC10. This was also assumed due to the non-uniform stress situation. Mapping of the test data worked very well with the simple model. Failure curve: closed.

TC11 : Laminate IM7/8551-7, $\{\hat{\sigma}\} = (0,\ 0,\ \sigma_z,\ \hat{\tau}_{zy},\ 0,\ 0)^T$

Problem and Task: As before, just the lay-up is a cross-ply.

Comparison:

Due to the less fibre orientations this stack has less critical locations than TC10. Therefore, as confining crushing stress, $\hat{\sigma}_z^{cr} = -1100 MPa$ was assumed. Further, as the model cannot involve stack differences and the result − consequently − is equal for TC11 and TC10, the higher load-carrying capacity of TC11 was considered by a factor computed of the ratio $1100/1000$ of the assumed crushing strengths.

- A very good mapping could then be obtained with the simple strength model.

TC12 : Laminate IM7/8551-7, $\{\hat{\sigma}\} = (0,\ 0,\ \sigma_z,\ 0,\ 0,\ 0)^T$

Problem: Effect of the applied surface pressure $\sigma_z = -p$ on the average fracture strains: in-plane normal strains $\hat{\varepsilon}_x, \hat{\varepsilon}_y$ and through-thickness (out-of-plane) normal strain $\hat{\varepsilon}_z$. Curing stress from effective temperature: $\Delta T = -177° + 23° = -154°$: $\sigma_2^t = 22 MPa$.

Task: Determination of strain-stress curves $\hat{\varepsilon}_x(\sigma_z) = \hat{\varepsilon}_y(\sigma_z)$, and $\varepsilon_z(\sigma_z)$ of this waisted solid test specimen composed of a balanced symmetric cross-ply [0/90/0/90]ns

Comparison:

04.04.2014

At the high pressure domain of the curve, the UD material analysis comes to an end because the pre-requisite 'homogenized UD material' is violated. An approach was searched that captures the growing effect of a filament-upon-filament situation. This was considered by the simple approach of the non-linear increase of $E_\perp(\sigma_z)$, see section 4.3.

- Applying the Part A $E_\perp = 8400 MPa$, the bottom curve is predicted. The curve shows a stiffness increase due to the Birch effect. However, as the Birch effect needs a micro-mechanical treatment, a correction factor had to be employed because micro-mechanical data and formulas are not compatible. This has been performed for all three curves.
- The filament-upon-filament progressive fracture situation was captured by Eq.(11). Then, the course of the Part B test data could be well mapped.
- The computation indicates initiation of wedge failure IFF2 at about $-400 MPa$. Then, IFF2-fracture is delayed due to friction under the piston and also by the filament-upon-filament situation. It leads to filament notching accompanied by an increasing FF1 danger which finally will generate fracture beyond $\sigma_z^{max} = -1400 MPa$.

6 Conclusions

6.1 Relevance of results to design practice

Usually, bi-axial and tri-axial compression brings a beneficial increase of load-carrying capacity. This can be utilized in structural domains where such situations are encountered. *Physically-based, lamina-oriented* and *validated* 3D failure conditions are the tools to use these benefits in design engineering.

Principally, just the lamina test cases TC2 through TC7 are directly applicable for validating the FMC *failure conditions* including tri-axial pressure behaviour of the matrix investigated in TC1 whereas the laminate test cases TC8 through TC12 can only serve for verification of the full *failure theory*. In each TC the investigation of the influence of wall-thickness on hoop stress is mandatory.

Based on functional and operational requirements often design limits are posed in terms of deformation or as design limit strains. Therefore, serviceability might limit the application. Further, a fully crushed laminate has usually no practical value because it can only compressed but not tensioned again. Of course, one may try to simulate this special '*structural*' failure (no real material failure anymore, according to the FMC) behaviour of the laminate beyond the applicability limit of *material* strength failure conditions in order to obtain more confidence in the non-linear theory. Thereby, one should not forget the much lower size of the design limit strain of usually $\varepsilon_{design} \equiv \varepsilon_\parallel \equiv \varepsilon_\perp < 0.5\%$

Another fact, also linked to structural failure, is that for $R_\parallel^c$ practically never a real material strength value is measured. Using a waisted coupon test specimen and an accurate test procedure the compressive value is practically the same as the tensile value, $R_\parallel^c = R_\parallel^t$ [Ban10]. This indirectly impacts many TCs.

Some specific points and facts can be dedicated to the Test Cases:
TC1 :
- In the hydrostatic domain, for this dense matrix an open failure surface exists

- No 2^{nd}Tg-effect found was demonstrated by the test data, even more the opposite tendency was obvious. Therefore, unfortunately matrix behaviour and 2^{nd}Tg-effect modelling, which would have to be built up in TC1, could not be substantiated for the mandatory use in several of the following Test Cases. TC is just informative for design.

TC2, TC3, TC4 :

- Sufficient test data was provided to use the results and to benefit in shear stress dominated designs when high pressures are acting such as at the anchors of tension cables of bridges. Only the 90° values can be directly used for design purposes, but not the 0° tube values (see *Annex 4*).

TC5 :

- As the lower branch in quadrant III could be mapped and the upper branch indirectly by the literature, the obtained results can be used in design.

TC6 , TC7 :

- The sudden drop in quadrant IV can be not explained. The Poisson effect seems to be ruled out at medium pressures after being over-emphasized at small pressures. Experiments are required which capture a domain until about $-800 MPa$. This means the work of Hine should be completed in order to clarify the discrepancy in the curvatures of the two branches. A remark on benefits for the design cannot be given.

TC8, TC9 :

- TC8: Results may be used in design practice as, with the simple non-linear MathCad program, values on the conservative side are computed in the provided test data domain.
- TC9: Within the technical domain of < 0.5% fracture strain the results can be used for design purpose.

TC10, TC10, TC12 :

- TC10, TC11: Despite of the fact that mapping could be achieved the results cannot be generalized for design purpose.
- TC12: The provided 'similar' data set could be well mapped after increasing the stiffness due to the fact that fibres will come to lie upon another after a distinct surface compression. The results are not applicable for the usual structural design but give a hint upon the risk in a final extreme loading case. No further use is possible with such a 'squeezed' laminate.

Some basic conclusions:

* Generally, it is physically not accurate to predict a failure surface with the knowledge of strength data only! Friction is inherent with brittle behaving materials and to be considered.

* In contrast to a dense isotropic material a dense UD material might fracture under a very high hydrostatic compression stress ($\sigma = -p_{hyd}$), according to the Poisson effect which makes the filament strain (TC5) to reach the fracture strain $e_{\parallel}^{c} = p_{hyd} \cdot (1 - 2 \cdot v_{\perp\parallel}) / E_{\parallel}$, that means under the pre-requisite $2 \cdot v_{\perp\parallel} < 1$

* Higher load carrying capacity or resistance, obtained under p_{hyd}, is the result of the favourably affected equivalent stress σ_{eq}. It's not from an increasing technical strength $\overline{R}$

Experimental results can be far away from the reality like a bad theoretical model. Theory creates a model of the reality, 'only' and one experiment is 'just' one realisation of the reality.

6.2 Issues with the model

* FMC-based failure conditions, as one part of a failure theory, are proven to be valuable tools in 2D (WWFE-I) and in 3D situations, so far too, and need not to be modified. Gaps in the provided data sets and the quality of the data do not demand to think about FMC-based UD model modifications. A model does not capture all the test data, and not all the current test data can be captured by a given model. In this context it is essential that the provided test data deliver no argument to change the model. They just affect the value of the model parameters.

* Modelling in the high non-linear domain (large deformation, large strain) is not sufficiently stabile performed by the used MathCad program, but this was usually outside of the engineering range. Problems with convergence in the iteration loops were encountered in TC8 and TC9. If a commercial FEA code can be used the non-linear behaviour is professionally captured in contrast to the author's program, however the FMC is not yet implemented in a commercial code. Using such a FE code, the result of a less good failure condition might be equalized by a better non-linear coding and vice-versa.

Through-thickness material behaviour of unidirectional and multi-directional laminates is more complex that the in-plane response of composites.

In structures, composed of stiff fibres and fibre-dominated designed by netting theory, the fibre net controls the strain behaviour. This makes modelling pretty linear and simple.

* Above the initial failure level an appropriate progressive failure analysis method has to be employed by taking a *Successive Degradation Model* and by using a failure mode condition that indicates failure type and quantifies damage danger or fracture risk, respectively. The FMC considers the intra- and the inter-laminar stresses and grades the activated failure modes. Therefore, associated degradation models are inherent and make a gradual degradation of the affected property possible, which accompanies the damage evolution.

* Loading path effects considering the consecutive IFF in the laminate have not been considered but require some investigation. Deterministic failure path and probabilistic failure path of a laminate may not coincide with each other, still due to the possibility of having different scatter ranges of the design parameters. This is essential for hybrids.

* A novel idea is the treatment of TC2, 3 and 4. The first point is the distinction of redundant and isolated behaviour. Using this, no mapping problems in the vicinity of the abscissa existed anymore. The second point is the idea with the determination of the average stress-strain curve. This made it possible, that in all the three curves the physically given 'check point' is consistently located.

6.3 Filling gaps in the test data

* There were several sources of error besides the errors that directly happen to occur in the challenging tests. These are the evaluation of raw test data, placing of test data in the graph, quality of the test data. Encouraging the quality of test data is a permanent task

* Lack in tests data domains: Only well understood testing and material behaviour, coupled with a careful evaluation of the raw test data can verify the assumptions made and validate a model. The provided test results cover a wide range of 3D stress combinations, but it remains quite a lack of data in certain areas. Due to this lack of knowledge, questionable test data could not be discussed or possibly re-evaluated.

 * The strain-hardening branch can be fitted on basis of the provided properties, whereas the strain-softening branch of embedded laminas (post-initial failure, embedded properties) with characterization of the lamina's in-situ behaviour must be assumed. Necessary for the non-linear analysis procedure of the laminate are the secant moduli $E_\perp^c$ and $G_{//\perp}$ in both the regimes. further investigation of the successive failure and degradation of the embedded lamina is necessary in order to confirm the results published in [Kno03]. This must be viewed in the context of sorting out a general transferability to a lamina in any laminate of a family. In this context should be checked whether the real fracture strain will increase due to ' p_{hyd} - healing' because failure is no more a weakest link problem. Besides the approach above, continuum and fracture mechanics approaches are also applied.

* 2^{nd}Tg-effect in higher hydrostatic work cases: The effect reduces the slope of the curves of the elasticity moduli and the resistance ('strengths'). Both the properties show an increase of the associated curve under p_{hyd}. A full modelling of the matrix behaviour under p_{hyd} was not possible for the author because TC1 test data do not exhibit the necessary information. Also, the following TCs do not show a clear 2^{nd}Tg-effect. The effect is not yet well understood due to missing knowledge and literature shows discrepancies. What has been done in Part A and B was pure guessing. To better understand this phenomenon that is active beyond $p_{hyd} = 200 MPa$ some physical properties should be measured. This addresses experiments to determine the elasticity moduli degradation, major Poisson's ratio $\nu_{\perp\parallel}(p_{hyd})$, and the degradation of the multi-axial 'strength' slopes as well, see the experiments of Pae and Shin. In the test programme, tests should be included with different stresses in the three coordinate directions (p_{hyd} means equal stress values).

6.4 Understanding failure phenomena and terms

* The first FF in case of mass-optimized laminates (fibre-dominated laminates) means final failure, if the laminate is not over-dimensioned. So, usually FF in at least one lamina of a laminate means final failure of the laminate. Therefore, the biaxial failure envelopes for final failure of laminates predicted by various theories do not differ that much, as long as the laminates have three or more fibre directions. Also, the predicted stress/strain curves of such laminates look very similar because the fibres which are much stiffer than the matrix carry the main portion of the loads. Different degradation procedures after the onset of inter-fibre failure (IFF) do therefore not influence the predicted strains very much. This is especially true for CFRP laminates.

* *Initial failure* (onset of failure) and *final failure* is indicated by a loss in stiffness which is indicated by a kink and a drop in the load. Failure by IFF is always indicated in the figures but marking final failure is a problem whenever strong non-linearity occurs, such as large deformation or large strain. For instance, the solid compression-loaded TC12 will not fall apart under compressive σ_z^c. The squeezed laminate carries higher and higher load, however,

just for compression, but a structural part cannot be used anymore after this situation. Engineers must define *What is physical failure, especially final failure?* based on the task the structural part has to fulfil. The maximum through thickness stress $\sigma_z^{max} = -1400 MPa$ may be defined final fracture or not. *Final failure* occurs after the structure has degraded to a level where it is no longer capable of carrying additional load. This is most often caused by FF, however in specific cases by an IFF, too. For instance, the wedge-shaped inter-fibre crack (IFF2) can lead to final failure if it damages the neighbouring layers by its capability to 'notch' and cut filaments in the neighbouring laminas to finally cause delamination.

* Inescapably, as theoretical *failure load* is taken the maximum load achieved when computation stops due to numerical stability problems in non-linear analysis which might be very much below reaching failure.

* It is discriminated *material failure* (strength *failure condition* as one part of a *failure theory is* applicable) from *structural failure* of a crushing tube.

* In general, non-linear analysis results in a *stress-redistribution* within the thickness of a laminated *structure*. This redistribution lowers, due to diffuse and later discrete micro-cracking, the matrix-dominated stress level including the residual stresses in the laminae of the laminate. Residual stresses in a lamina of the laminate are released (decay) due to decreasing stiffness caused by the degradation which accompanies increasing non-linearity.

* In CLT analysis, the applied lamina stresses are *sme*ared over a length that includes some micro-cracks generated after the onset of IFF until final failure of the laminate. A roof sign marks an average laminate stress.

* The *effective mode strength* of an embedded lamina is higher, than that of the mode strength (i.e. $\overline{R}_\perp^t$) which is measured by *isolated* specimens. The value is not a 'weakest link result' (series failure system) as given in case of the isolated specimen but a 'redundancy result' (parallel failure system) or an *in-situ* value due to embedding of the lamina in the laminate.

* *Mixed (strength) failure* behaviour occurs if a distinct stress state activates several failure modes. Then, the failure behaviour becomes mixed.

 * Multidirectional laminates are usually still capable of carrying a 2D-loading beyond *initial failure* which usually is determined by IFF. For 3D-loading (i.e.TC10) this is different.

 * Transversal bi-axial compression of a UD specimen causes, due to the constraining fibres, a 3D compression state of stress in the matrix material.

6.5 Use of FMC-based strength failure conditions in case of little knowledge

  - Each single failure condition needs just the associated mode strength of that mode which is activated by the multi-axial stress state. The necessary strength value (for UD, at maximum 5) always must be known for design.

  - Friction values (2D: 1 value $\mu_{\perp\parallel}$; 3D: 2 values $\mu_{\perp\parallel}, \mu_{\perp\perp}$) can be assessed.

   A value $\mu = 0$ means no friction, which is on the safe side. As the usual CFRP with a duroplastic polymer is brittle a value of 0.1 is recommended.

  - Under bi-axial and tri-axial compression the knowledge of the major Poisson's ratio ν_{12} is mandatory, but this value is known from design, anyway.

Result: The application is possible without any problems in pre-design. Missing model parameters are just a problem if validation is aimed at.

Acknowledgement

References

[Ban10] Bansemir H.: Presentation at CCeV, WG Engineering, Nov. 18, 2010, Augsburg. CCeV (Carbon Composites e.V.)-website

[Bec94] Becker W. and Kress G.: Stiffness Reduction in Laminate Coupons due to the Free-edge Effect. Comp.Science and Technology 52 (1994), 109-115

[Bel1885] Beltrami E.: Sulle Condizioni di Resistenza dei Corpi Elastici. Rend. ist. d. sci. lett., Cl. mat. nat.18, 705-714 (1885)

[Bir38] Birch R.: The Effect of Pressure Upon the Elastic Parameters of Isotropic Solids, according to Murnaaghan's Theory of Finite Strains. Journal of Applied Physics 9 (4), 279-288.

[Bro94] Brown T.L. and Hyer M.W.: Effects of layer waviness on the stresses and failure in hydrostatically loaded cylinders. Jan 1994, Paper ID STP24333S, Digital library / STP / STP1185-EB / STP24333S; 17 pages

[Cad78] Caddell R.M., Raghava R.S. and Atkins A.G.: Pressure dependent yield criteria for polymers. Materials Science and Engineering 13 (1978), 113-120

[Cun04a] Cuntze R.G. and Freund A: The Predictive Capability of Failure Mode Concept-based Strength Criteria for Multidirectional Laminates. Part A, Composites Science and Technology 64 (2004), 343-377

[Cun04b] Cuntze R.G.: The Predictive Capability of Failure Mode Concept-based Strength Criteria for Multidirectional Laminates. Part B, Composites Science and Technology 63 (2004), 487-516

[Cun07] Cuntze R.G.: Prediction of Static 3D and In-plane Fracture Failure of UD Laminas composed of Fibre-reinforced Plastics. 4th NAFEMS Nordic Seminar on Materials's Modelling, Sandvika, March 2007, Conference CD

[Cun10] Cuntze R.G.: The Predictive Capability of Failure Mode Concept-based Strength Conditions for Laminates composed of UD laminas under Static Tri-axial State of stresss. WWFE-II, Part A, to be issued in Composites Science and Technology, Elsevier

[DeTer99] DeTeresa, S.J.: Failure of a composite lamina under three-dimensional stresses. UCRL-JC-135664

[DeTer04] DeTeresa S.J., Dennis, C., Freeman O.C., and Groves S.E.: The Effects of Through-thickness Compression on the Interlaminar Shear Response of Laminated Fibre Composites. J. Compos Mater, V 38, No. 8, pp681-697, 2004

[DeTer01] DeTeresa S. J, Allison L.M., Freeman O.C., and Groves S.E.: Matrix-dominated Performance of Thick-Section Fibre Composites for Flywheel Applications. Society for the Advancement of Material and Process Engineering 2001 Symposium, Long Beach, CA., May 5-10, 2001

[Fla82] Flaggs, D.L. and Kural, M.H.: "Experimental Determination of the In Situ Transverse Lamina Strength in Graphite Epoxy Laminates". J. Comp. Mat. Vol 16 (1982), 103-116

[Hine05] Hine, P.J., Duckett, R.A., Kaddour, A.S., Hinton, M.J., and Wells, G.M.: The effect of hydrostatic pressure on the mechanical properties of glass fibre/epoxy unidirectional composites. Composites Part A, 2005, 279-289

[Hin04] Hinton, M.J., Soden, P.D. and Kaddour, A.S.: Failure criteria of fibre reinforced polymer composites. The World-Wide Failure Exercise. Elsevier, 2004, ISBN 0-08-044475-X, 700 pages

[Hin10] Hinton, M.J. and Kaddour, A.S.: Tri-axial Test Results for Fibre-Reinforced Composites-Second World-Wide Failure Exercise Benchmark Data. Information, January 2010

[Hop95] Hoppel, C.R.R., Bogetti, T.A. and Gillespie, J.W.jr.: Literature review – Effects of hydrostatic pressure on the Mechanical Behaviour of Composite Materials. J. of Thermoplastic Composite Materials 8 (1995), 375-409

[Hye88] Hyer, M.W.: Hydrostatic response of thick laminated composites cylinders. J. of Reinforced Plastics and Composites 7, 1988, No 4, 321-340

[Kad09] Kaddour, A.S. and Hinton, M.J.: Instruction to Contributors of the Second World-Wide Failure Exercise (WWFE-II) , Part B

[Kad10] Kaddour A. S., Thompson L., Li S., and Hinton M.J.: Through-thickness compressive behaviour of carbon/epoxy laminates'. to be published

[Kad10b] Kaddour A.S., Soden P.D., and Hinton M.J.: Effect of through-thickness compressive stress on the bi-axial compressive strength of 55° E-glass/epoxy tubes. to be published

[Kno03] Knops, M.: Sukzessives Bruchgeschehen in Faserverbundlaminaten. Dissertation 2003. Aachen, Institut für Kunststoffverarbeitung (IKV)

[Kre07] Kress G.: Finite-Element Modeling for Simulating Strength Testing with Tubular Specimens. NAFEMS Seminar "Simulating composite materials and structures", Bad Kissingen, Nov. 2007

[Liu95] Liu W., Soden P.D., and Kaddour A.S.: Design of end plugs for specimens under external pressures. Computers and Structures, V 83, pp 976–988, 2005.

[13] Michaeli, W. and Lambrecht, L.: *Neue Software für realitätsnahe Auslegung von Laminaten*. Lightweight design 4, 2010, pp. 4.2- 4.8

[Pae96] Pae, K.D.: Influence of Hydrostatic Pressure on the Mechanical Behaviour and Properties of Uni-directional, Laminated, Graphite fibre/Epoxy matrix, Thick Composites. Composites Part B 27B (1996), 599-611

[Pae77] Pae, K.D.: The macroscopic yielding behaviour of polymers in multi-axial stress fields. J. of Materials Science 12 (1977), 1209-1214

[Par81] Parry T. V., and Wronski A. S.: Kinking and tensile, compressive and interlaminar shear failure in carbon fibre reinforced plastics beams tested in flexure. J Mater Sci, Vol. 16, pp. 439-450, 1981

[Par82] Parry T.V., and Wronski A.S.: Kinking and compressive failure in uniaxially aligned carbon fibre composite tested under superimposed hydrostatic pressure. J Mater Sci, Vol. 17, pp. 893-900, 1982

[Par90] Parry T.V., and Wronski A..S.: 'The effect of hydrostatic pressure on the transverse strength of glass and carbon fibre epoxy composites. J. Mater Sci, Vol. 25, pp3162-3166, 1990.

[Par85] Parry, T.V. and Wronski, A. S.: The effect of hydrostatic pressure on the tensile properties of pultruded CFRP. J. of Materials Science 20 (1985), no. 6, pp 2141-2147

[Puc02] Puck A. and Schuermann H.: Failure Analysis of FRP Laminates by Means of Physically based Phenomenological Models. Composites Science and Technology 62 (2002), 1633-1662

[Rhe95] Rhee, K.Y. and Pae, K.D.: Effects of Hydrostatic Pressure on the Compressive Properties of Laminated, 0° Unidirectional, Graphite Fibre/Epoxy Matrix Thick-Composites. J. of Composite Materials,Vol.29, No.10, 1995, pp.1295-1307

[Rhe01] Rhee, K.Y.: Deformation characteristics of multi-directional carbon fibre/epoxy composites under high pressure. Polymer composites 22, 2001, (6)

[Rhe04] Rhee, K.Y., Lee and Park: Effect of hydrostatic pressure on the mechanical behaviour of sea-water-absorbed carbon-epoxy composite. Materials Science and Engineering A, Vol. 384, issues 1-2, Oct 2004, pp. 308-313

[Rol97] Rolfes, R., Noor, A.H. and Rohwer, K.: Efficient Calculation of Transverse Stresses in Composite Plates. MSC-NASTRAN User Conference, 1997

[Shi92a] Shin, E.S. and Pae, K.D.: Effects of hydrostatic pressure on the torsional shear behaviour of graphite/epoxy composite. Journal of Composite Materials, 28 ,1992 , No 4, 462-485

[Shi92b] Shin, E.S. and Pae, K.D.: Effects of hydrostatic pressure on in-plane shear properties of graphite-epoxy composites. J. of Composite Materials, Vol. 26, no. 6, 1992, pp. 828-868

[Tsa71] Tsai, S.W. and Wu, E.M. A General Theory of Strength for An-isotropic Materials. Journal Comp. Materials 5 (1971), 58-80

[VDI2014] VDI 2014: German Guideline, Sheet 3 "Development of Fibre-Reinforced Plastic Components, Analysis". (in German and English. Beuth Verlag, 2006)

[Wro82] Wronski A.S. and Parry T.V.: Compressive failure and kinking in uniaxially aligned glass-resin composite under superimposed hydrostatic pressure. J Mater Sci, Vol. 17, pp3656-3662, 1982.

Annex 1: FMC-based Fracture Failure Modes and Strength Failure conditions

An equivalent stress σ_{eq} includes all stresses that are acting together in a given mode. The vector of the modes' equivalent stresses reads

$$\{\sigma_{eq}^{mode}\} = \left(\sigma_{eq}^{\|\sigma},\ \sigma_{eq}^{\|\tau},\ \sigma_{eq}^{\perp\sigma},\ \sigma_{eq}^{\perp\tau},\ \sigma_{eq}^{\|\perp}\right)^T . \tag{A1}$$

Employing the mode *strength* $\overline{R}^{mode}$, its *equivalent stress* σ_{eq}^{mode}, and Eq.(13) - according to the general equation $Eff^{mode} = \sigma_{eq}^{mode} / \overline{R}^{mode}$ - the following set of formulas for the material stressing effort of each of the 5 modes can be provided and its relationship to the associated equivalent stress:

FF 1 $\quad Eff^{\|\sigma} = \breve{\sigma}_1 / \overline{R}_\|^t = \sigma_{eq}^{\|\sigma} / \overline{R}_\|^t \qquad$ with $\quad \breve{\sigma}_1 \cong \varepsilon_1^t \cdot E_\|$ (matrix negligible),

FF 2 $\quad Eff^{\|\tau} = -\breve{\sigma}_1 / \overline{R}_\|^c = +\sigma_{eq}^{\|\tau} / \overline{R}_\|^c \qquad$ with $\quad \breve{\sigma}_1 \cong \varepsilon_1^c \cdot E_\|$, $\qquad$ (A2a-e)

IFF 1 $\quad Eff^{\perp\sigma} = [(\sigma_2 + \sigma_3) + \sqrt{(\sigma_2 - \sigma_3)^2 + 4\tau_{23}^2}]/2\overline{R}_\perp^t = \sigma_{eq}^{\perp\sigma} / \overline{R}_\perp^t$,

IFF 2 $\quad Eff^{\perp\tau} = [b_{\perp\perp} \cdot \sqrt{(\sigma_2 - \sigma_3)^2 + 4\tau_{23}^2} + (b_{\perp\perp} - 1) \cdot (\sigma_2 + \sigma_3)] / \overline{R}_\perp^c = +\sigma_{eq}^{\perp\tau} / \overline{R}_\perp^c$

IFF 3 $\quad Eff^{\perp\|} = \{[\sqrt{b_{\perp\|}^2 \cdot I_{23-5}^2 + 4 \cdot \overline{R}_{\perp\|}^2 \cdot (\tau_{31}^2 + \tau_{21}^2)^2} + b_{\perp\|} \cdot I_{23-5}]/(2 \cdot \overline{R}_{\perp\|}^3)\}^{0.5} = \sigma_{eq}^{\perp\|} / \overline{R}_{\perp\|}$

$$\text{with} \quad I_{23-5} = 2\sigma_2 \cdot \tau_{21}^2 + 2\sigma_3 \cdot \tau_{31}^2 + 4\tau_{23}\tau_{31}\tau_{21} \tag{A3}$$

and as friction parameters $b_{\perp\|} \equiv \mu_{\perp\|}$, $b_{\perp\perp} \cong 1/(1 - \mu_{\perp\perp})$ with the friction values of the UD material, measured as shown in Part A. Typical ranges: $0 < \mu_{\perp\|} < 0.3$, $0 < \mu_{\perp\perp} < 0.2$ (the extremely high value $\mu_{\perp\|} = 0.56$, asked to be applied in WWFE-I TC1, was not correct as a later test data investigation of the author backs up). In Part B, $b_\perp^\tau$ was renamed as $b_{\perp\perp}$ because this is now in line with a fully symbolic indexing. Of course, the friction parameters can be also determined by simulation of the course of test data (Eqs.7 and 8 in WWFE-II, Part A). In the case of certain compressive stress ratios σ_3 / σ_2 the equivalent stress or the respective material stressing effort $Eff^{\Diamond\tau}$ can become negative. Such a negative value physically means that IFF2 will not occur due to strong friction. For numerical reasons such a problem is by-passed by setting $x = (x + |x|)/2$. The second part in IFF2 and in IFF3 is the effort reducing friction part. The magnitude of this part $(b_{\perp\perp} - 1) \cdot (\sigma_2 + \sigma_3)$ should remain − w.r.t. the 3D validity of the model- below the $b_{\perp\perp} \cdot \sqrt{(\sigma_2 - \sigma_3)^2 + 4\tau_{23}^2}$.

Above stresses include the nonlinearly load-dependent load stresses $\{\sigma\}_L$ and the equally nonlinearity dependent residual stresses $\{\sigma\}_R$ from curing etc.

Notes: (1) Each failure mechanism is affected by an associated typical state of stress. The failure mechanism with the highest material stressing effort will dominate the failure. The mode effort has to become zero if the mode driving stress is zero. (2) Due to IFF the curing stresses decay in parallel to the degradation. (3) The non design-driving stresses of a mode might increase or decrease the material stressing effort which is basically caused by the design driving one. This influence is considered in the

equivalent mode stress $\sigma_{eq}^{\text{mode}}$. (4) The 5 strength and 2 friction parameters can be measured and therefore fulfil a basic design verification requirement: Strength properties shall be statistically-based, material friction properties μ are so-called physical quantities which shall be average (typical) values. (6) The FFs are special fibre strain failure equations. (7) In elastic cases, where the stress is proportional to the load, the material stressing effort is the inverse of the (material) reserve factor. (8) The Mises equivalent stress for the mode yielding is not the only equivalent stress.

An interaction of the failure modes has to be executed due to the fact that the full failure surface consists of five parts. Cuntze models the interactions of them by a simple probabilistically based 'series spring model' approach [Cun04, Rac87]. Such a model describes the lamina failure system as a series failure system which fails whenever any of its elements fails. Each mode is one element of the failure system and is seen to be independent of the others. The series spring model was proposed as engineering approach because it approximates the results of a time-consuming probabilistic interaction calculation on the safe side. By this method, the interaction between FF and IFF modes as well as between the various IFF modes acts - in these 'mixed' failure domains - as a rounding-off procedure linked to the determination of the desired values for the resultant material stressing effort *Eff* . This effort automatically takes into account the interactions between all the affected modes by summing up all the proportionate mode material stressing efforts

$$Eff^{\,m} = (Eff^{\,\|\sigma})^m + (Eff^{\,\|\tau})^m + (Eff^{\,\perp\sigma})^m + (Eff^{\,\perp\tau})^m + (Eff^{\,\perp\|})^m \qquad \text{for UD} \qquad \text{(A4)}$$
$$= 1 = 100\% \text{ , if failure.}$$

In other words, the interaction equation includes all mode material stressing efforts and each of them represents a portion of load-carrying capacity of the material. At maximum, in thin laminas, 3 modes of the 5 modes will physically interact. Considering 3D-loaded thick laminas, there, all 3 IFF modes might interact together with one FF.

For using Eq.(16) a value for the interaction exponent *m* is to be provided. Usually, the value of *m* is obtained by curve fitting of test data in the interaction zone. FRP mapping experience delivered that *2.4 < m < 3*, at least for CFRP. This mode interaction exponent *m* is also termed rounding-off exponent, the size of which is high in case of low scatter and vice versa. As with other interaction equations, for *m* it is also valid: a lower value chosen for the interaction exponent is more on the safe side.

Note: As a simplifying engineering assumption, m is always given the same value, regardless of the distinct mode interaction domain considered! This spring model is applied for every other interaction in Part B, too.

Annex 2: Enabling an Automatic Use of the Failure Conditions in 3D Applications

In order to make an automatic use of the FMC-based fracture failure conditions also in a 3D state of stresses possible and to avoid complicate queries in the computer program some specifica are of interest or were introduced:

1) FF1, IFF1, IFF2: By the automatic insertion of a state of stress physically incorrect negative efforts and equivalent stresses may occur. This can be bypassed by the Föppl-Macauley brackets which represent the equations

$$\langle Eff^{\|\sigma} \rangle = (\varepsilon_1 + |\varepsilon_1|) \cdot E_\| / (2 \cdot R_\|^{\,t}) , \quad \langle Eff^{\|\tau} \rangle = (-\varepsilon_1 + |\varepsilon_1|) \cdot E_\| / (2 \cdot R_\|^{\,c}) , \text{ and}$$

04.04.2014

$$\left\langle \sigma_{eq}^{\perp\sigma} \right\rangle = (+\sigma_{eq}^{\perp\sigma} + \left| \sigma_{eq}^{\perp\sigma} \right|)/2 \ , \quad \left\langle \sigma_{eq}^{\perp\tau} \right\rangle = (+\sigma_{eq}^{\perp\tau} + \left| \sigma_{eq}^{\perp\tau} \right|)/2 . \tag{A5}$$

A negative $\sigma_{eq}^{\perp\tau}$ may occur in the case of a combination of a high friction parameter $b_{\perp\perp}$ with a certain state of bi-axial stressing.

2) IFF3: When deriving Eq.(A2e) no *proportional stressing* (all stresses are changed by the same factor) was applied to all stresses but just to the failure driving shear stresses. This practically affects the interaction domain, only, which is dominated by m .

3) IFF1, IFF2: In order to avoid a problem in automatic insertion of the 3D failure conditions in numerical analysis this paragraph has been added. The problem is originated by the fact that a shear stress τ_{23} can be composed by a normal tensile stress with a normal compressive stress. This affects two failure modes but just one is significant in the case of the actual, brittle behaving UD material. Due to this, naturally a tensile effort (driving effort in case of a brittle behaving material) $Eff^{\perp\sigma}$ is caused and a compressive effort $Eff^{\perp\tau}$ as well. As the compressive effort incorporates a small additional failure danger this is considered via the principal stresses in the quasi-isotropic $x_2 - x_3$ domain (additional advantage: reduction to two stress parameters = principal stresses)

$$\sigma_I = 0.5 \cdot (\sigma_2 + \sigma_3) + \sqrt{(0.5 \cdot (\sigma_2 - \sigma_3))^2 + \tau_{23}^2} \ , \tag{A6}$$

$$\sigma_{II} = 0.5 \cdot (\sigma_2 + \sigma_3) - \sqrt{(0.5 \cdot (\sigma_2 - \sigma_3))^2 + \tau_{23}^2}$$

with $\sigma_I : 0$ if $\sigma_I \geq 0$, σ_I otherwise, and $\sigma_{II} : 0$ if $\sigma_{II} \geq 0$, σ_{II} otherwise. Then it holds

$$Eff^{\perp\tau} = [\ b_{\perp\perp} \cdot \sqrt{\sigma_I^2 - 2 \cdot \sigma_I \cdot \sigma_{II} + \sigma_{II}^2 + 4 \cdot 0^2} + (b_{\perp\perp} - 1) \cdot (\sigma_I + \sigma_{II})\ ]\ / \bar{R}_\perp^c . \tag{A7}$$

From the above failure condition can be seen that the principle stresses work identically. This causes the two solution branches in the respective TCs. By the procedure above, also tensile stresses are tackled which cause a problem when being automatically inserted into IFF2.

4) IFF2: Solving Eq.(A2d) $Eff^{\perp\tau} = 1$ for $\sigma_2(\sigma_3)$ will deliver two roots and therefore two branches as can be seen in case of TC 5, for instance.

04.04.2014

Annex 3: Provided Mechanical Properties of the UD laminas

Fibre type	IM7	T300	A-S	S2-glass	E-Glass
Matrix	8551-7	PR-319	Epoxy1	Epoxy2	MY750
Fibre volume fraction V_f (%)	60	60	60	60	60
Longitudinal modulus E_1 (GPa)	*165**	*129*	*140**	*52*	*45.6*
Transverse modulus E_2 (GPa)	*8.4*	*5.6+*	*10*	*19*	*16.2*
Through-thickness modulus E_3 (GPa)	8.4	5.6+	10	19	16.2
In-plane shear modulus G_{12} (GPa)	*5.6**	*1.33+*	*6**	*6.7**	*5.83**
Transverse shear modulus G_{13} (GPa)	5.6*	1.33+	6*	6.7*	5.83*
Through-thickness shear modulus G_{23} (GPa)	2.8	1.86	3.35	6.7	5.7
Major Poisson's ratio υ_{12}	*0.34*	*0.32*	*0.3*	*0.3*	*0.28*
Major transverse Poisson's ratio υ_{13}	0.34	0.32	0.3	0.3	0.28
Through-thickness Poisson's ratio υ_{23}	*0.5*	*0.5*	*0.49*	*0.42*	*0.4*
Longitudinal tensile strength X_T (MPa)	*2560*	*1378*	*1990*	*1700*	*1280*
Longitudinal compressive strength X_C (MPa)	*1590*	*950*	*1500*	*1150*	*800*
Transverse tensile strength Y_T (MPa)	*73*	*40*	*38*	*63*	*40*
Transverse compressive strength Y_C (MPa)	*185***	*125***	*150***	*180***	*145***
Through-thickness tensile strength Z_T (MPa)	63	40	38	50	40
Through-thickness compressive strength Z_C (MPa)	185**	125**	150**	180**	145**
In-plane shear strength S_{12} (MPa)	*90***	*97***	*70***	*72***	*73***
Transverse shear strength S_{13} (MPa)	90**	97**	70**	72**	73**
Through-thickness shear strength S_{23} (MPa)	57	45	50	40	50
Longitudinal tensile failure strain ε_{1T} (%)	*1.55*	*1.07*	*1.42*	*3.27*	*2.81*
Longitudinal compressive failure strain ε_{1C} (%)	*1.1*	*0.74*	*1.2*	*2.21*	*1.75*
Transverse tensile failure strain ε_{2T} (%)	*0.87*	*0.43*	*0.38*	*0.33*	*0.246*
Transverse compressive failure strain ε_{2C} (%)	*3.2*	*2.8*	*1.6*	*1.5*	*1.2*
Transverse tensile failure strain ε_{3T} (%)	0.76	0.43	0.38	0.263	0.25
Through-thickness compressive failure strain ε_{3C} (%)	3.2	2.8	1.6	1.5	1.2
In-plane shear failure strain γ_{12u} (%)	*5*	*8.6*	*3.5*	*4*	*4*
Transverse shear failure strain γ_{13u} (%)	5	8.6	3.5	4	4
Through-thickness shear failure strain γ_{23u} (%)	2.1	1.5	1.5	0.59	0.88
Longitudinal thermal coefficient α_1 (10^{-6}/°C)	-1	-1	-1	8.6	8.6
Transverse thermal coefficient α_2 (10^{-6}/°C)	18	26	26	26.4	26.4
Through-thickness thermal coefficient α_3 (10^{-6}/°C)	18	26	26	26.4	26.4
Energy release rates G_{Ic}, G_{IIc} (J/m^2 = 1N/m)	200				240, 1500
mixed (fracture mechanics) mode to be assumed					
Stress free temperature (°C)	177	120	120	120	120
Test Case	TC10,11,12	TC2,3,4	TC7	TC6	TC1,5,8,9

* Initial modulus.
** Nonlinear behaviour and stress strain curves and data points are provided
\+ These values are considered to be low, compared with typical data for the same material published somewhere else or quoted by the manufacturers. We have not attempted to change them in order to facilitate a comparison with test data in Part B.

Annex 4: 3D Stress-strain Relationship of Lamina and Laminate

$$\begin{Bmatrix} \varepsilon_1 \\ \varepsilon_2 \\ \varepsilon_3 \\ \gamma_{23} \\ \gamma_{13} \\ \gamma_{12} \end{Bmatrix} = \begin{bmatrix} \dfrac{1}{E_\parallel} & \dfrac{-v_{\parallel\perp}}{E_\perp} & \dfrac{-v_{\parallel\perp}}{E_\perp} & 0 & 0 & 0 \\ \dfrac{-v_{\perp\parallel}}{E_\parallel} & \dfrac{1}{E_\perp} & \dfrac{-v_{\perp\perp}}{E_\perp} & 0 & 0 & 0 \\ \dfrac{-v_{\perp\parallel}}{E_\parallel} & \dfrac{-v_{\perp\perp}}{E_\perp} & \dfrac{1}{E_\perp} & 0 & 0 & 0 \\ & & & \dfrac{1}{G_{\perp\perp}} & 0 & 0 \\ & & & & \dfrac{1}{G_{\parallel\perp}} & 0 \\ & (symm.) & & & & \dfrac{1}{G_{\parallel\perp}} \end{bmatrix} \begin{Bmatrix} \sigma_1 \\ \sigma_2 \\ \sigma_3 \\ \tau_{23} \\ \tau_{13} \\ \tau_{12} \end{Bmatrix} , \qquad \text{(A7)}$$

$$\{n\}/t = [A]\cdot\{\varepsilon_{lam}\}. \qquad \text{(A8)}$$

Annex 5: TC3, investigation of 0°-tubes and comparison with 90°-tubes

Just 90°-test specimen data was provided in Part A. For completing the understanding of pressure dependency on the shear behaviour of composites, in Part B additionally, 0°-test specimen data was offered. From experience with WWFE-I TC2 was clear that the different stress situations between 0°-tubes and 90° tubes under torsion loading have to be investigated in order to sort out whether the 0° tubes are usable or not.

In the case of only hydrostatic loading a 0° tube initially experiences (good approach) $\sigma_{hoop} = \sigma_{rad} = \sigma_{ax} = -p_{hyd}$ $\sigma_{hoop} \equiv \sigma_3 = -p_{hyd}$, $\sigma_1 = \sigma_{ax} = -p_{hyd}$ and a 90° tube a varying $\sigma_{hoop} \equiv \sigma_1$ with $\int \sigma_1(r)\cdot dr = -p_{hyd}\cdot\pi(r_{out}^2 - r_{int}^2)$, and $\sigma_{rad} \equiv \sigma_3 = \sigma_2 = -p_{hyd}$.

This outlines a clearer stress situation for the 0° tube. As far as the angle is small the test results are simpler interpretable than those of the 90° tubes. But this is not anymore true when the larger angles at fracture are encountered. Then, the stresses have to be transformed due to the fact that shearing under torsion loading (see *Fig. 5*) turns the fibre direction and the lamina coordinate system is not anymore identical with the coordinate system of the tube. The state of stress, applied at significant angles, does not represent lamina stresses (material coordinate system) anymore but structural stresses

$$\{\sigma\} = (\sigma_x, \sigma_y, \sigma_z, \tau_{yz}, \tau_{zx}, \tau_{xy})^T \equiv (\sigma_{ax}, \sigma_{hoop}, \sigma_{radial}, 0, 0, \tau_{xy})^T , \qquad \text{(A9a)}$$

which have to be transformed into a 3D state of lamina stresses

$$\{\sigma\} = (\sigma_1, \sigma_2, \sigma_3, 0, 0, \tau_{21})^T = (\sigma_\parallel, \sigma_\perp, \sigma_z, 0, 0, \tau_{\perp\parallel})^T \qquad \text{(A9b)}$$

for the performance of a strength verification or for data mapping, respectively. Otherwise, one would compare apples and oranges when using 90° and 0° data in a mixed way.

In figure TC2 of the WWFE-I, such a transformation has been performed, however there, it was a simple 2D problem. Now here, for one 0° test point a transformation is performed by non-linear CLT analysis (see [Hin10]), via the relationship $\gamma\cdot L = R_0\cdot\widehat{\varphi}$, with γ the given

shear strain, $L = 14.24mm$ the gauge length, $R_0 = 4.57mm$ the outer radius of the tube, and $\widehat{\varphi} = \varphi \cdot (\pi/180°)$ the twist in radians). The following computation, using the relationship $\{\sigma\} = [T_\sigma]^{-1} \cdot \{\sigma'\} = [T_\varepsilon]^T \cdot \{\sigma'\}$ from [VDI2014], delivers the real lamina stresses

$$\sigma_\parallel = \sigma_x (\cos\varphi)^2 + \sigma_y (\sin\varphi)^2 + 2\tau_{xy} \cos\varphi \sin\varphi,$$

$$\sigma_\perp = \sigma_y (\sin\varphi)^2 + \sigma_x (\cos\varphi)^2 - 2\tau_{xy} \cos\varphi \sin\varphi, \quad (A10)$$

$$\tau_{\perp\parallel} = (-\sigma_x + \sigma_y) \cdot \sin\varphi \cdot \cos\varphi + \tau_{xy} \cdot ((\cos\varphi)^2 - (\sin\varphi)^2).$$

Just to give an impression, it is exemplarily compared one 0°-test point (full circle) with one 90°-test point at -300MPa. With Eq.(A8) and for a simple linear elastic model, taking non-linearity not into account in contrast to the WWFE-I -TC2, the stresses and stressing efforts

$$0° \text{ tube: from TC3: } (\sigma_x, \sigma_y, \sigma_z, \tau_{xy})^T = (-300, -300, -300, \ 123)^T \ MPa, \ \varphi = 19.8°$$

$$\Rightarrow (\sigma_\parallel, \sigma_\perp, \sigma_z, \tau_{\perp\parallel})^T = (-222, -378, -300, \ 95)^T \ MPa \ ;$$

$$Eff_o = 0.78 \quad \text{from} \ \ Eff^{\parallel\tau} = 0.005, \ \ Eff^{\perp\parallel} = 0.78$$

are determined. This is to be compared to a 90° curve point (average) at $-300MPa$

$$90° \text{ tube: } \quad (\sigma_\parallel, \sigma_\perp, \sigma_z, \tau_{\perp\parallel})^T = (-300, -300, -300, \ 126)^T \ MPa \ ;$$

$$Eff_{90} = 1.08 \quad \text{from} \ \ Eff^{\parallel\tau} = 0.114, \ \ Eff^{\perp\parallel} = 1.08$$

and characterizes the two very different states of lamina stresses.

Conclusion:

A stress point of the 0°-data cannot be put into a diagram together with 90°-data. Therefore, they are not used in Part B. 90° tube test data can be 2D formulated as $\sigma(-p_{hyd}, \tau_{\perp\parallel})$ and thereby visualized by a 2D diagram, whereas for the 0° tube a 4D stress state (stresses are different, see above) is to be visualized. In the simple 2D-TC2 of WWFE-I this was still possible. Above coarse comparison further shows that the 0°-tube's twisting generates a reduced shear stress; equilibrium is achieved because the longitudinal fibres take over load. Remember that these 0° tubes are not wound but hot-press moulded.

Annex 6: Remarks on modelling of multi-fold material non-linearity

Besides the effort on the interpretation of the provided test data, a high effort was put at the modelling of the multi-fold material non-linearity. The latter effort addresses both the non-linear description of the secant moduli needed in the numerical analysis and the realistic consideration of interacting modes which produce an interaction damaging which is higher than for the added single portions. This interaction damaging or 'static damage accumulation' is to be respected.

The 'Mises' yield model 3D-describes one failure mechanism, whereas the multi-fold 'corner'-formulated Tresca model still requires approaches when the state of stresses lies in at the corners where a singularity prevails.

Generally, the application of the UD-IFF failure conditions requires the capture of three non-linear stress-strain curves. Pre-condition is the possibility to formulate equivalent stresses of a mode. A (quasi-)yield potential would lead to an equivalent strain $\varepsilon_{eq}^{mode}(\varepsilon_{ik})$, so that the stress-strain curve of the mode can be used as an equivalent stress-equivalent strain curve for non-linear modes such as IFF2 and IFF3.

04.04.2014

Finally, failure triggering in case of more than one failure causing mode needs to be investigated. This is very the same as with brittle isotropic materials.

* In order to implement the *multi-fold non-linearity* approach into a commercial FEA code, and taking advantage of the code's solution architecture w.r.t. non-linear laminate analysis, analogous to the isotropic input with *one mode yield condition + flow rule* for the *yield surface,* now a *multi-mode damage considering 'flow' rule* should be established for the *damage surface*. The interaction equation represents one basis for such an approach.

Figures

Fig. 1.

04.04.2014

Fig. 2.

Fig. 3

04.04.2014

stress at section
(fracture decisive)

$$\sigma = \sigma_1^{add} - p_{hyd}$$

external stress
applied at fracture

σ_1^{add}

$\sigma_3 = -p_{hyd}$

$\sigma_2 = -p_{hyd}$

p_{hyd}

Fig. 4.

M_t

90° fibres keep
90°orientation

0° fibres turn out of 0°direction

M_t

Fig. 5.

04.04.2014

Fig. 6.

04.04.2014
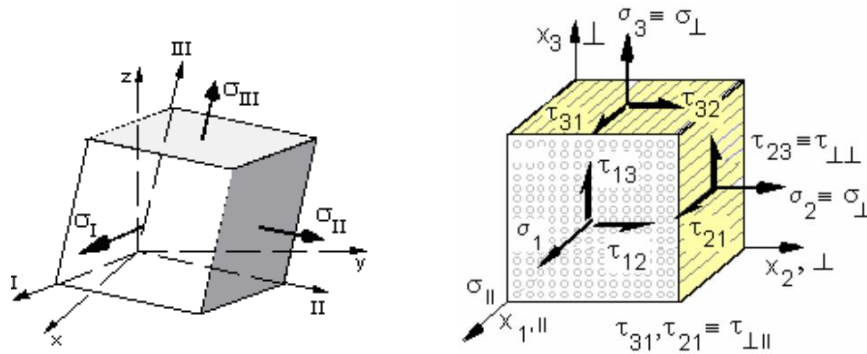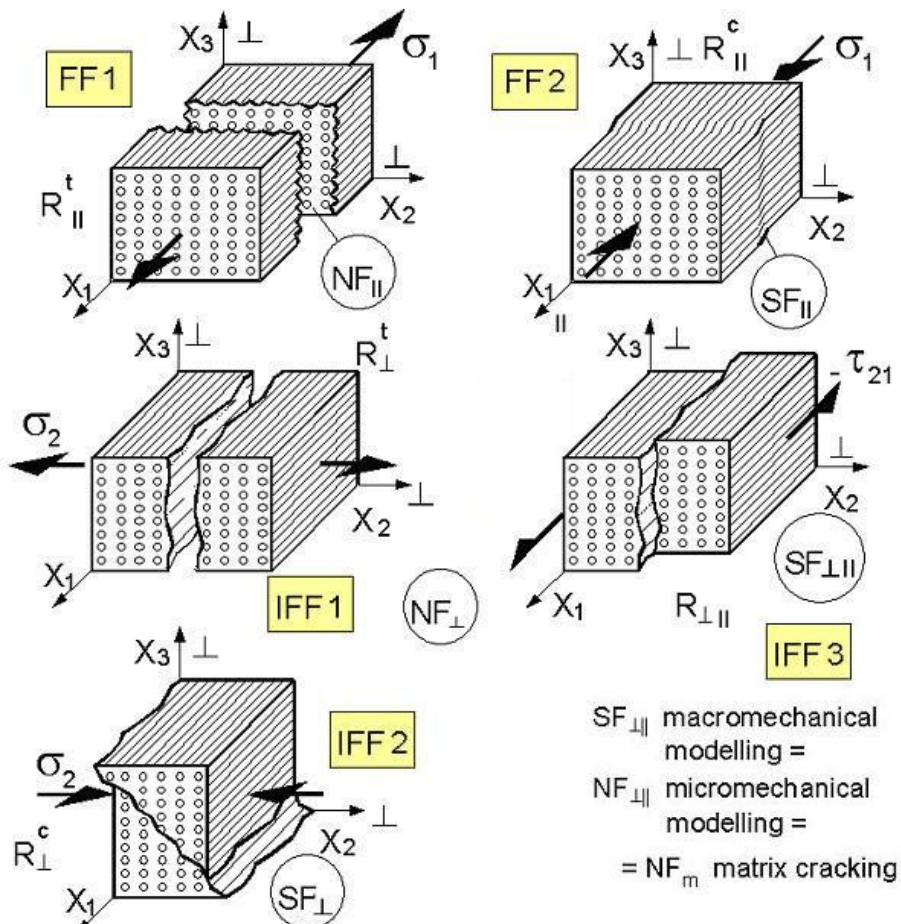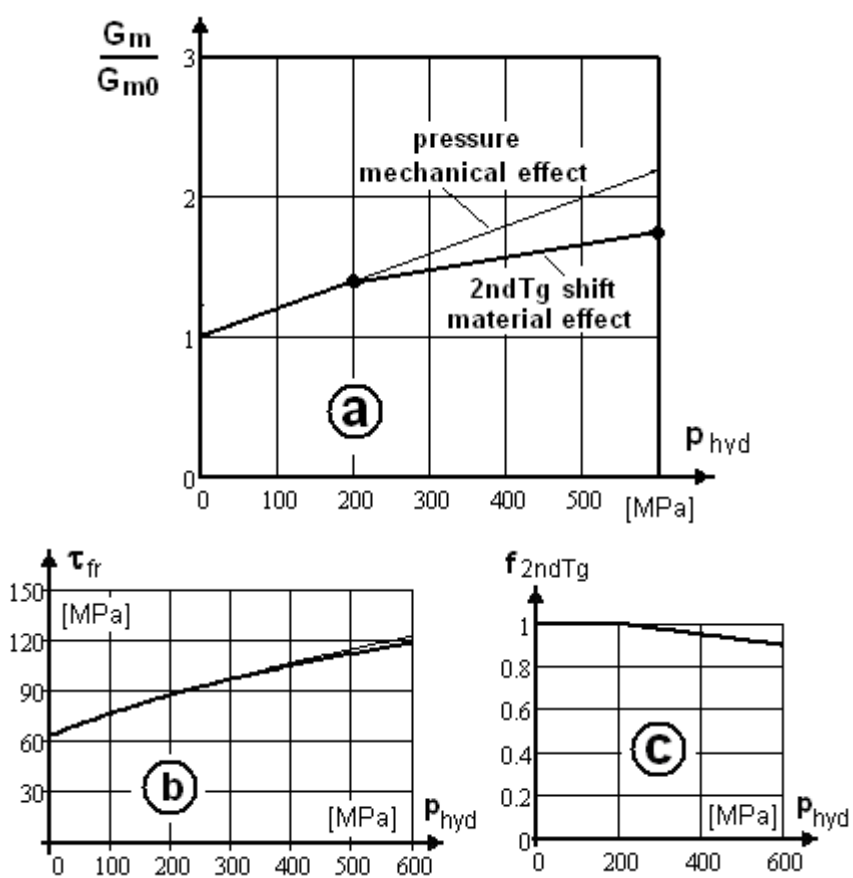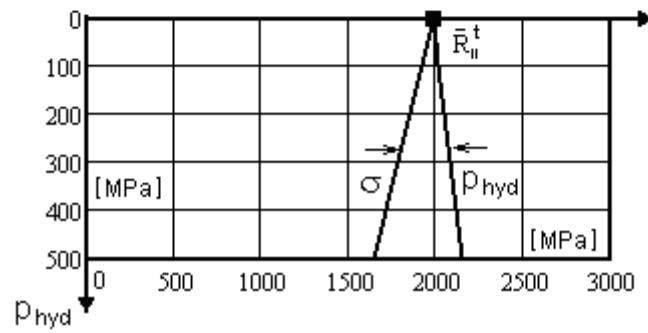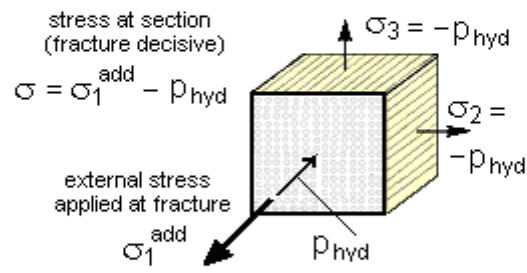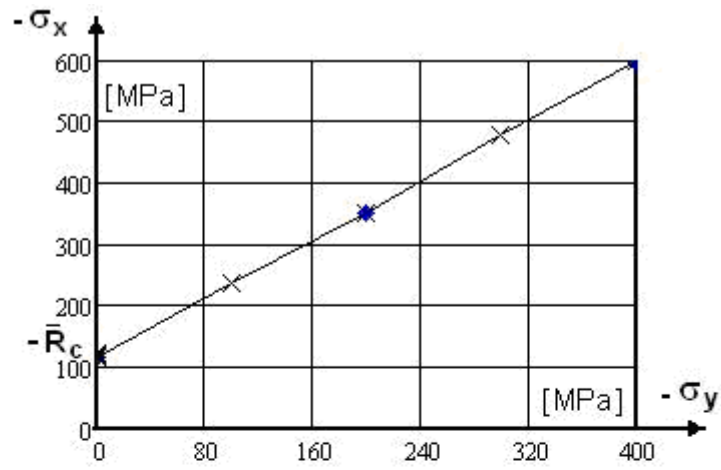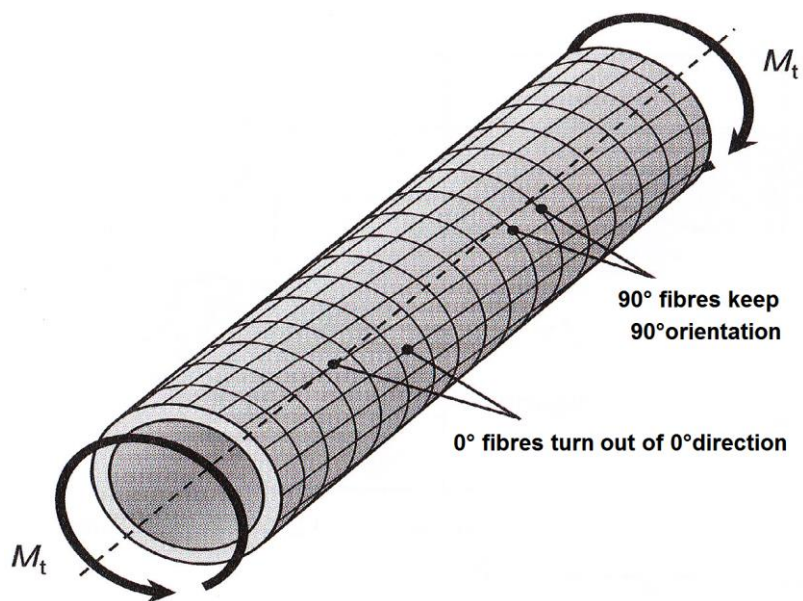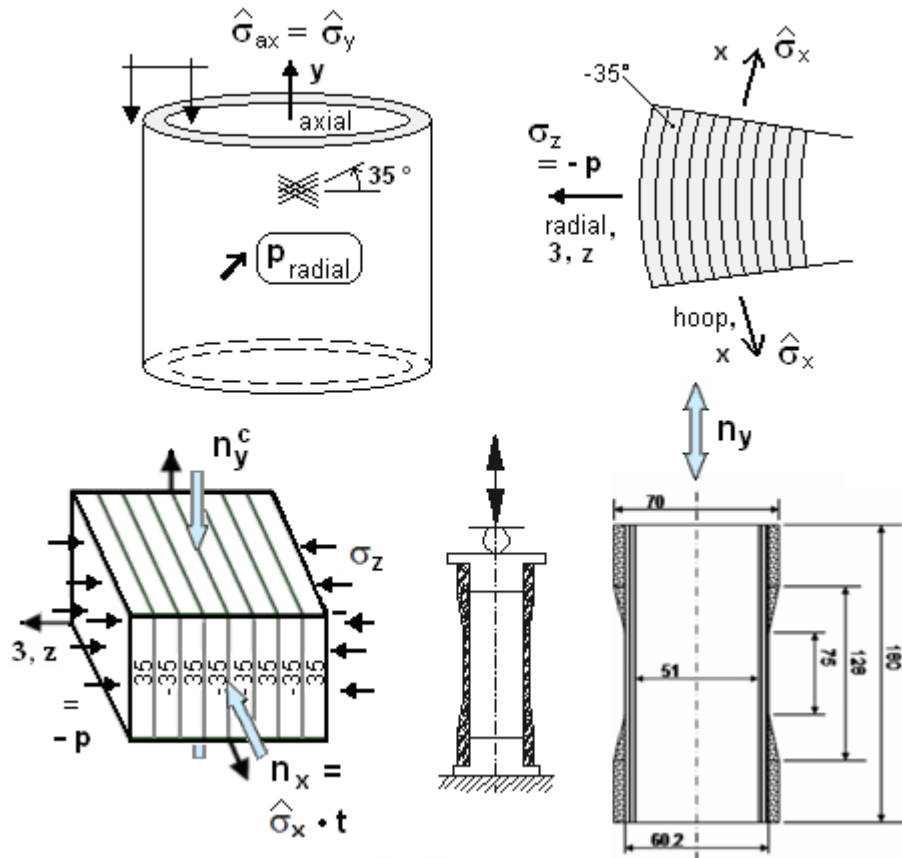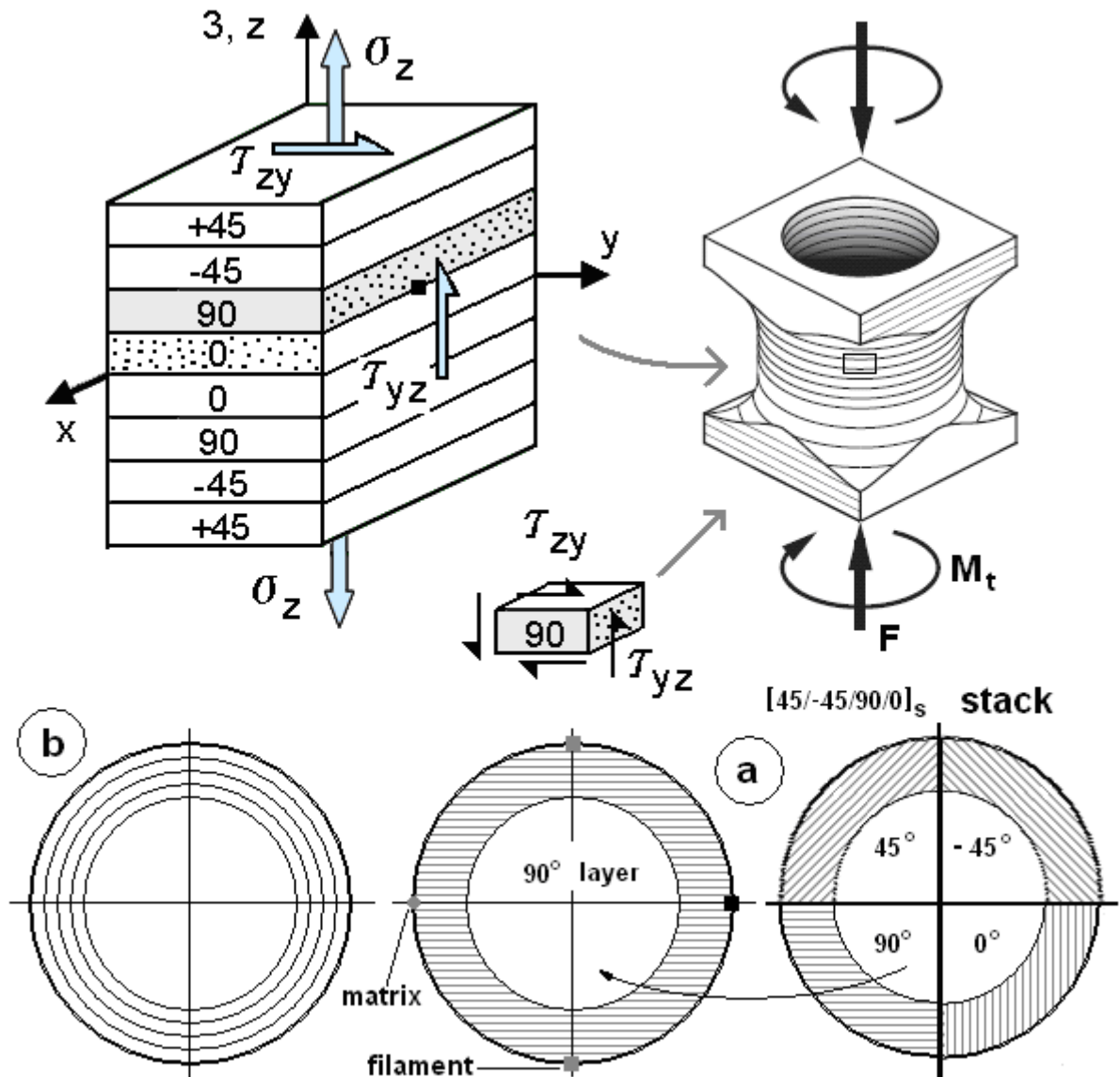
Fig. 7.

Table 1. Main features of the FMC and associated non-linear analysis

- Each *mode* represents one theoretically independent failure mechanism and one piece of the complete *failure surface* (surface of the failure body or so-called *limit surface*)
- Each failure *mechanism* is represented by one failure *condition*. One failure mechanism is governed by one basic strength and therefore has a clearly defined equivalent stress σ_{eq} and a *material stressing effort Eff* to be used at least in the (non-linear) progressive damage analysis
- An invariant formulation of a failure condition - in order to achieve a beneficial *scalar* formulation considering the material's symmetries - is possible
- For each *mode* one *material stressing effort* can be determined, displaying, where the design key has to be turned and linking highest material stressing effort to highest risk
- The invariant term in the failure condition can be related to a physical mechanism observed, when it causes a volume change or a shape change of the solid material element or 'internal friction'
- Curve-fitting of the course of test data is only permitted in each pure regime of a failure condition
- Rounding-off in mode interaction zones is performed by a spring model. This means a rounding-off of adjacent *mode failure curves* (*partial* surfaces) in their interaction zone which is leading again to a *global* failure curve (surface), or in other words, to a 'single surface failure description', such as with Tsai/Wu, however, without its well-known shortcomings
- Failure mode identification is mandatory for a progressive failure analysis in order to know how the lamina has failed. This makes a clear degradation of the moduli possible.
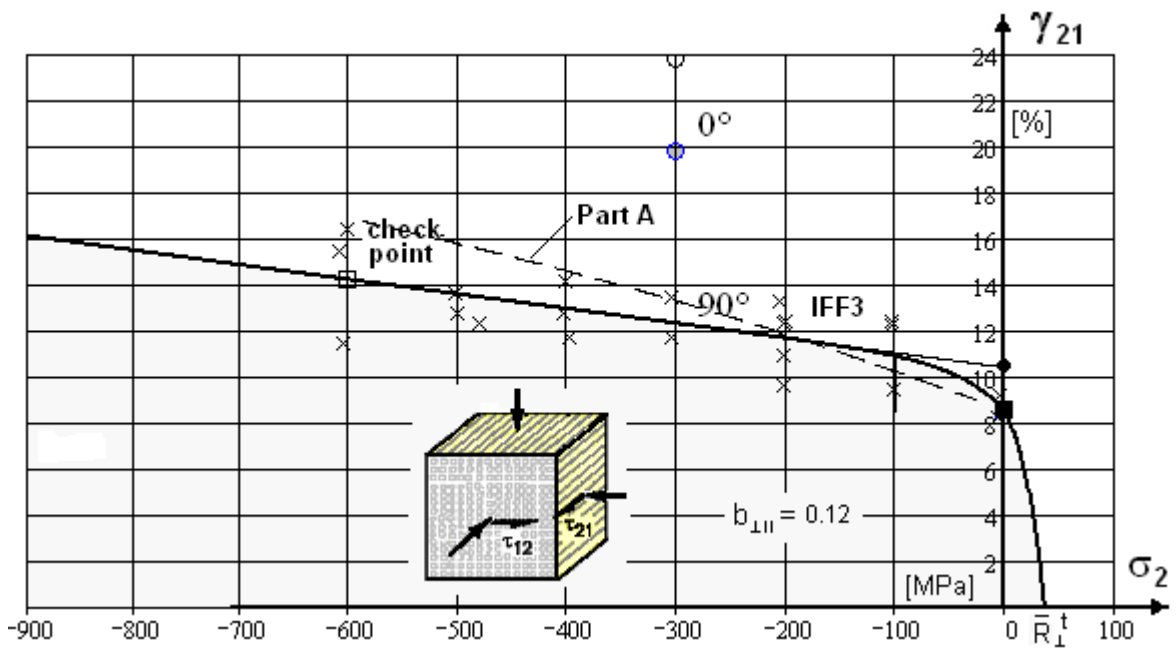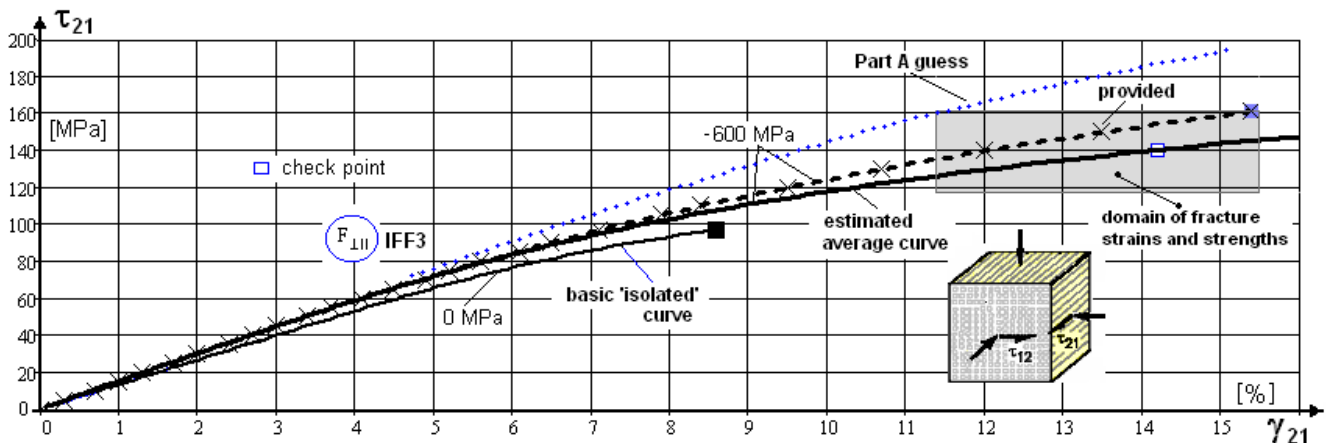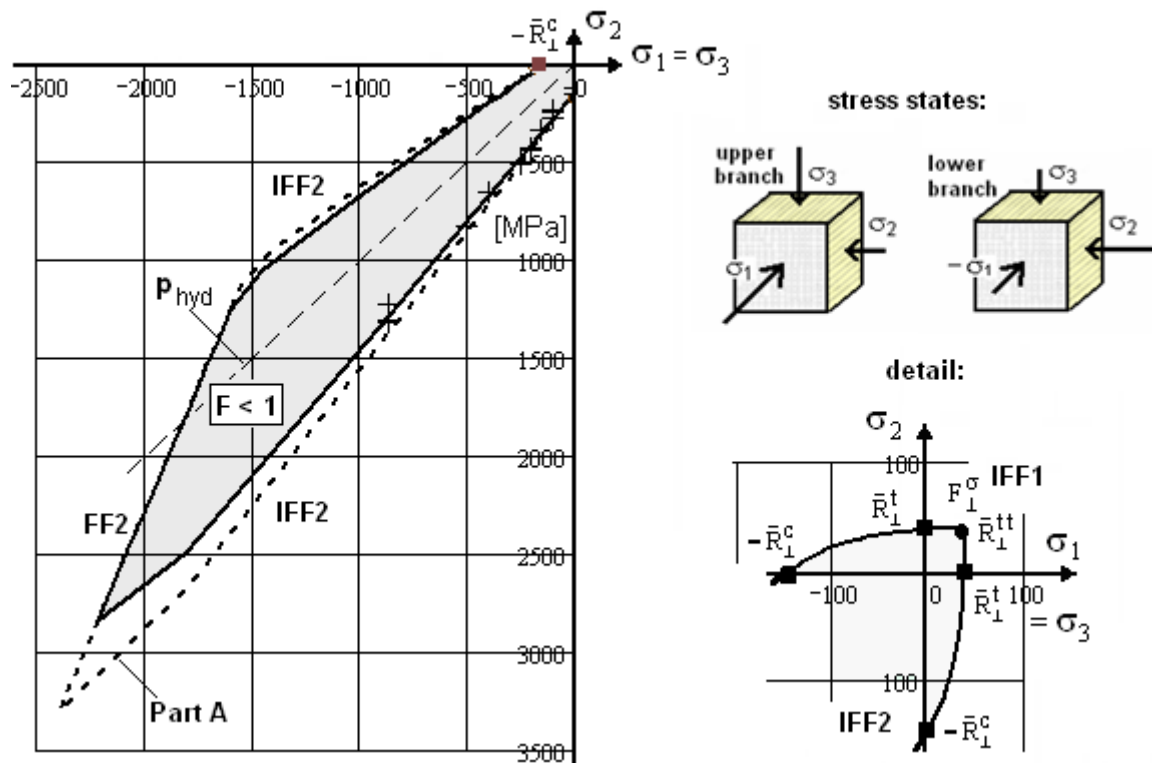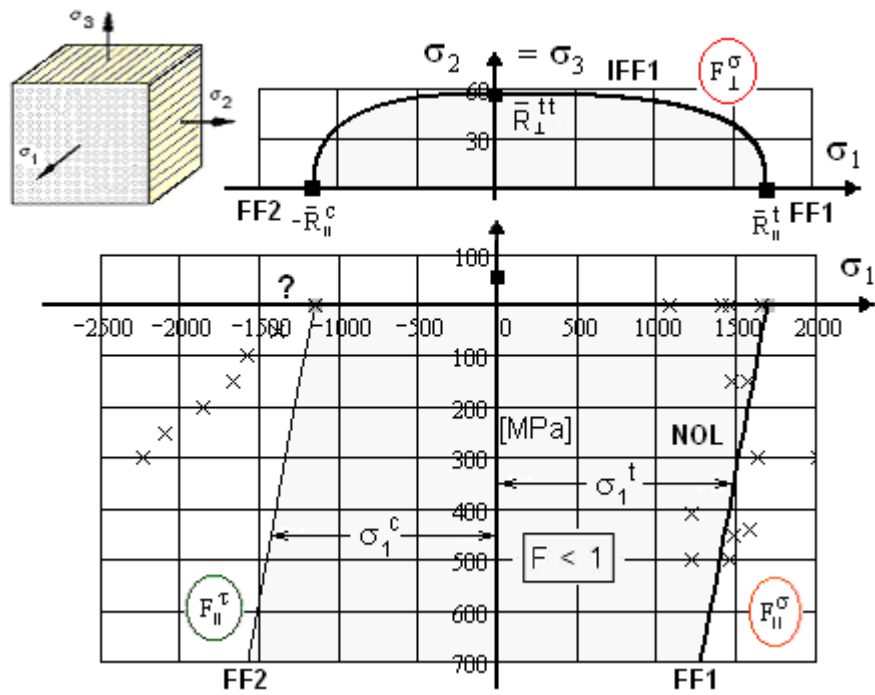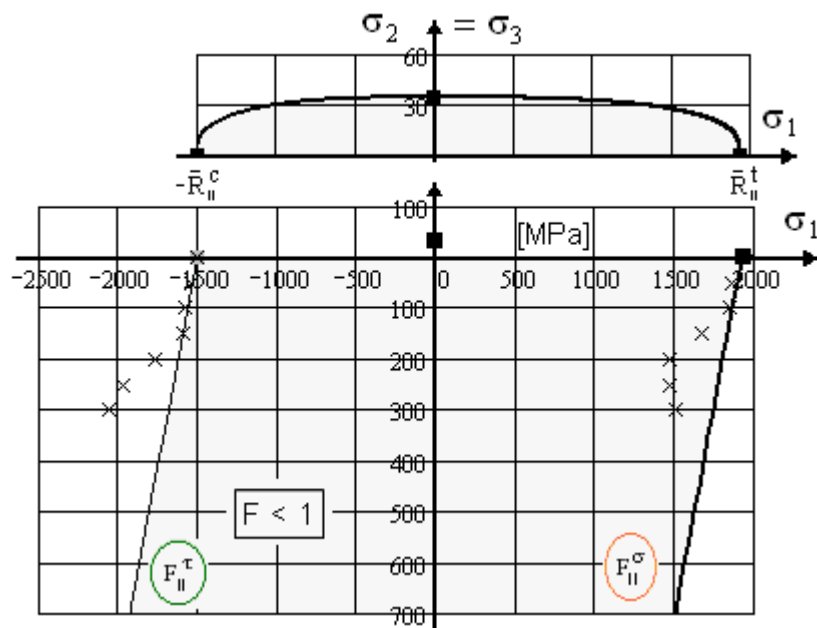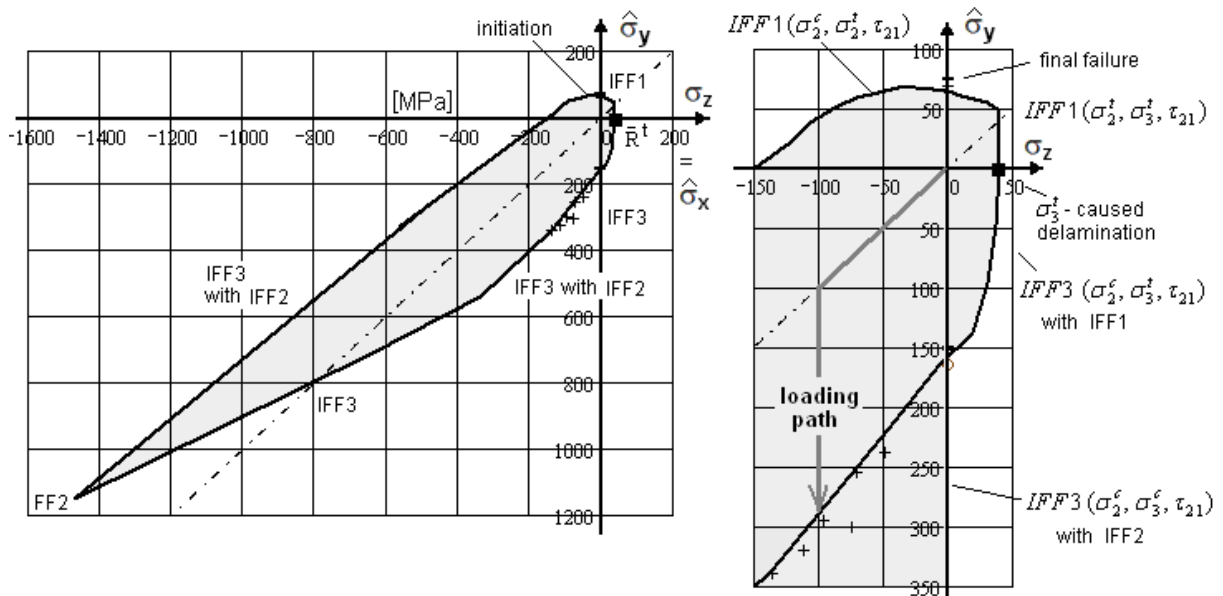
04.04.2014
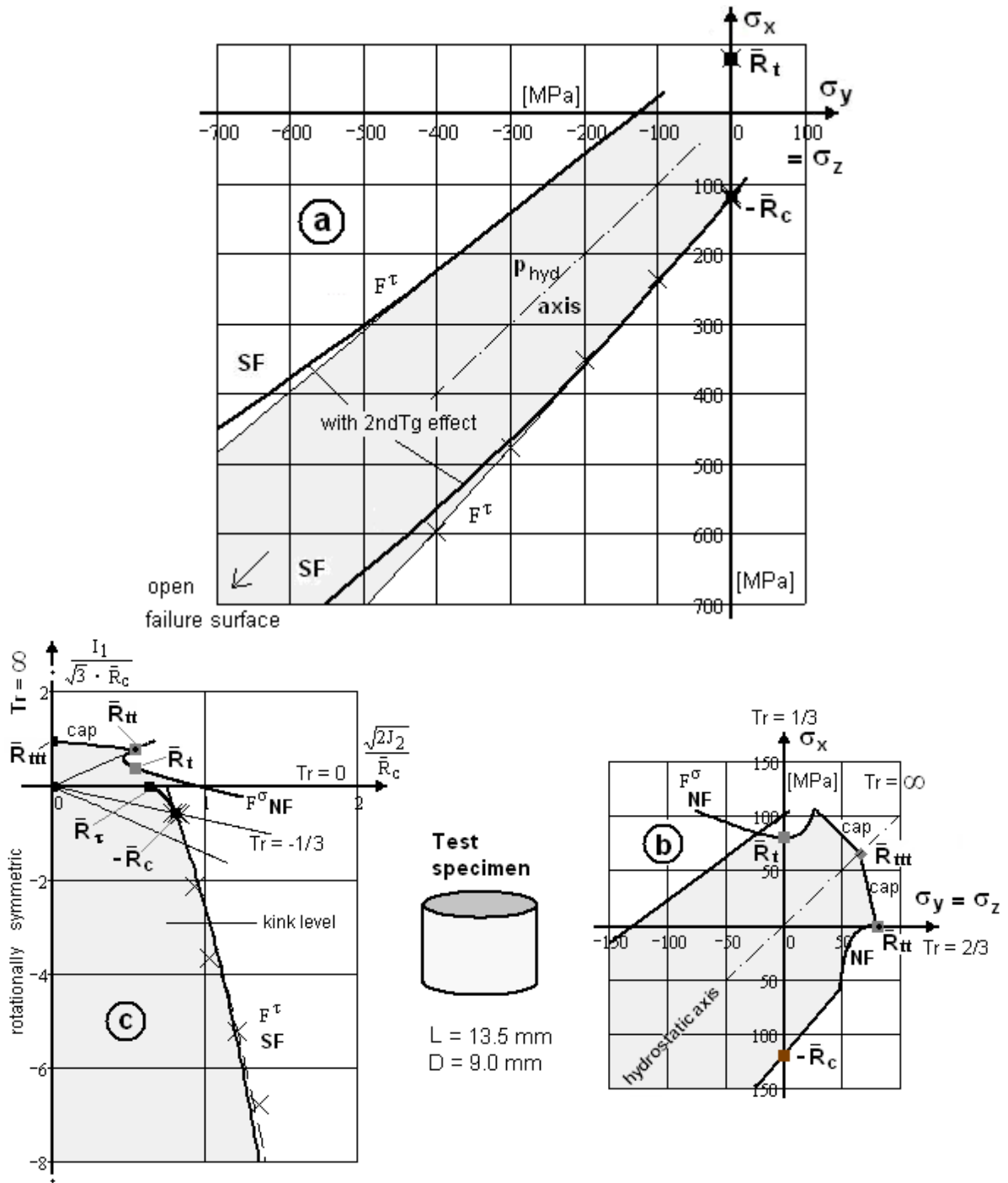
Figs. TC1.
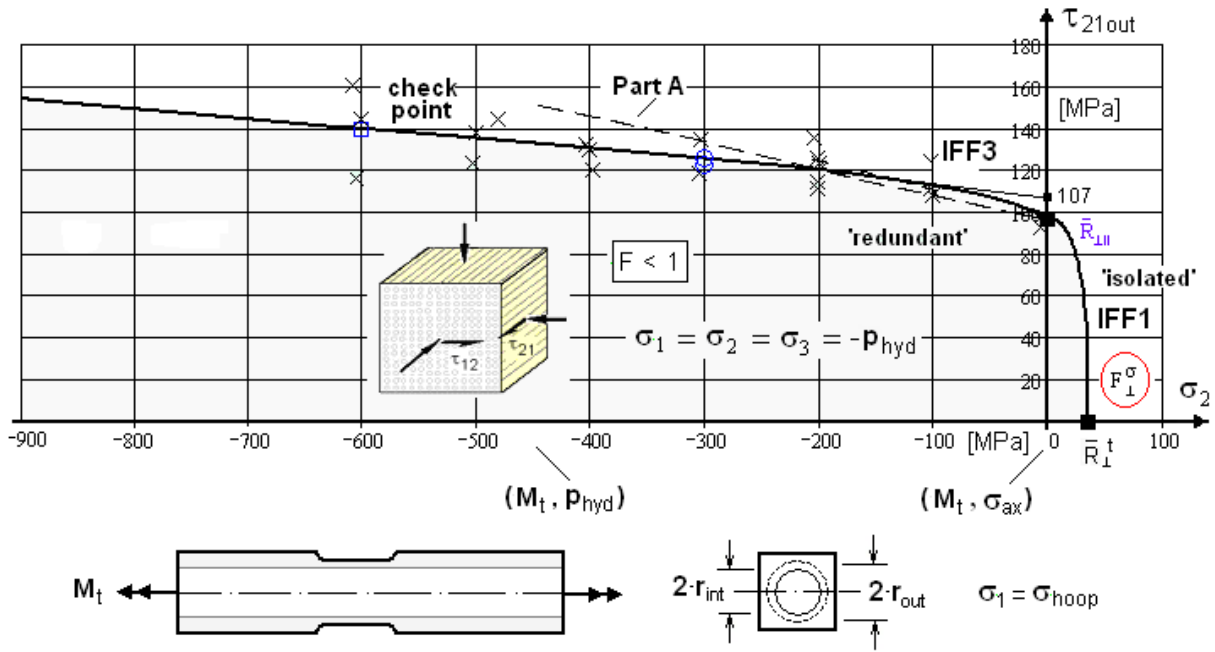
Fig. TC 2.

Fig. TC 3.

Fig. TC 4.

Fig. TC 5.

Fig. TC 6.

Fig. TC 7.

04.04.2014

Fig. TC 8.

Fig. TC 9

Fig. TC 10.

04.04.2014
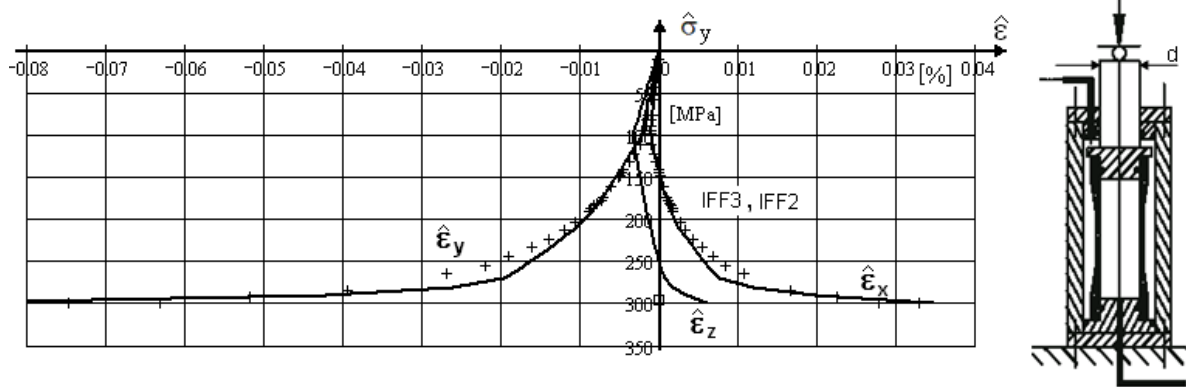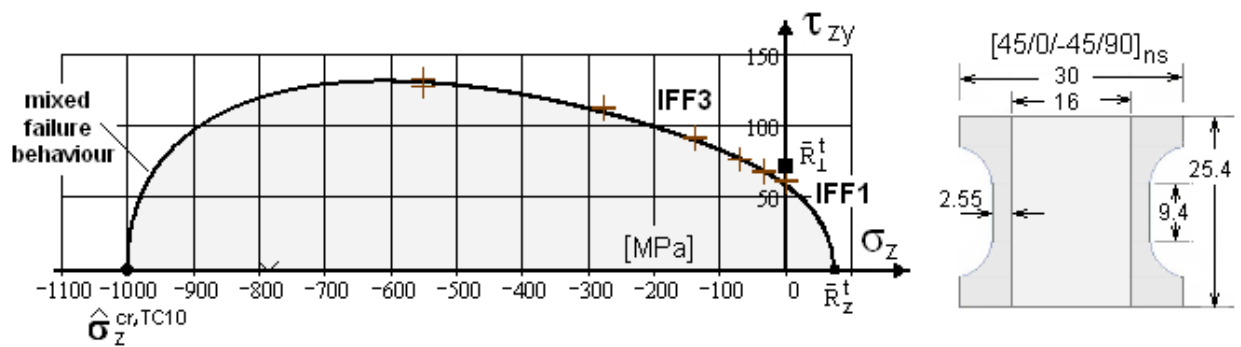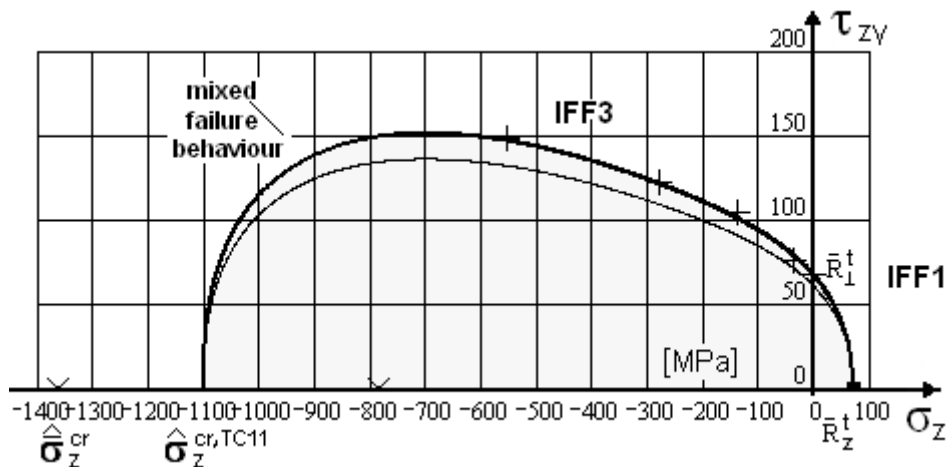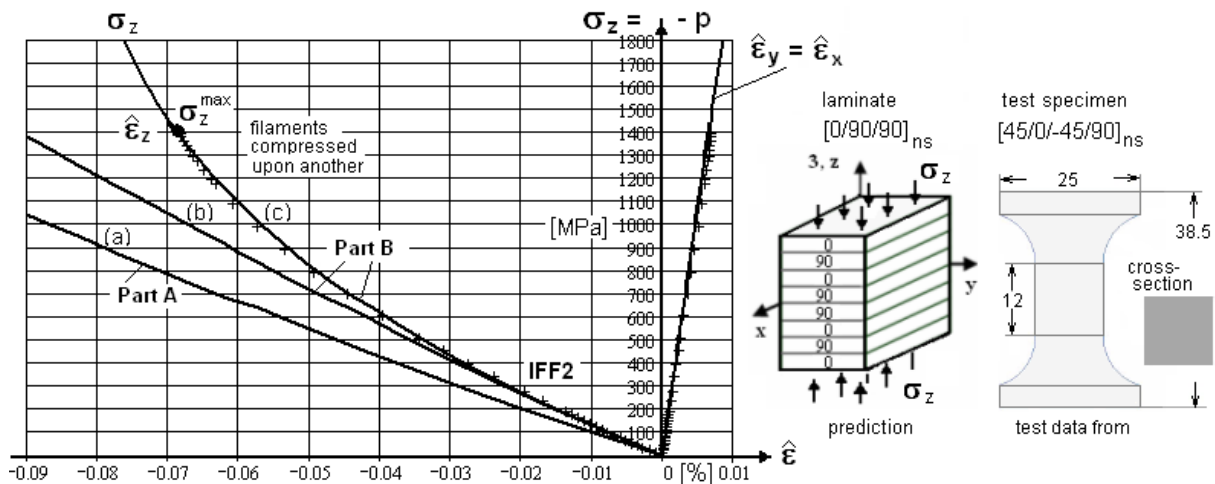
Fig. TC 11.

Fig. TC 12.

List of Figures and Tables

Fig. 1. Tri-axial state of stress, acting at a matrix material and a UD material cube.
For lamina coordinate and fibre orientation angle, see WWFE-II Part A

Fig. 2. FMC view of the fracture types of brittle transversely isotropic UD material.
NF:= Normal Fracture, SF:= Shear Fracture. Physical fracture "planes" are pointed out

Fig. 3.
(3a) 2nd Tg shift effect: Dependence of the matrix shear modulus on p_{hyd} . Assumption for PR319: knee point 200 MPa at ratio 1.4; final point 600 MPa at ratio 1.75, see [Pae96]).
(3b) Distribution of fracture stress.
(3c) Decay function f_{2ndTg} due to 2ndTg shift

Fig. 4. Transfer of experimental data in compressive and tensile domains. x = provided data, parallelogram = transformed data

Fig. 5. Change of the fibre orientation under torsion in TC2, TC3 (figure: courtesy of IKV Aachen)

04.04.2014

Fig. 6. Model of the TC8 test situation; $t_k = 0.25mm$, $t = 2mm$ laminate thickness

Fig. 7. TC10 modelling: (7a) shows a 90°-lamina of the stacked thick-walled tube milled from the sketched laminate block For comparison, (7b) shows the traditional wound or tape-layered tube

Figs. TC1. Tri-axial compressive failure stress curve $\sigma_{x,fr}(\sigma_y = \sigma_z)$ of the MY750 epoxy resin matrix, full cylinder, stress state $\{\sigma\} = (\sigma_x, \sigma_y = \sigma_z, \sigma_z, 0, 0, 0)^T$. $\{\overline{R}\} = (\overline{R}_t, \overline{R}_c)^T = (80, 120)^T MPa$, $R_\tau = 54MPa$, $b_\tau^c = 0.18$. $2^{nd}Tg$ shift effect: 10% slope decay of 'strength' curve assumed. Open failure surface

Fig. TC 2. Fracture stress $\tau_{21,fr}$ vs stress $\sigma_2(=\sigma_1 = \sigma_3 = -p_{hyd})$ for a UD T300 carbon/ PR319 epoxy hoop wound tube, $\sigma_{hoop} \equiv \sigma_1$, $\sigma_3 \equiv \sigma_{radial}$.
Check point: $\gamma_{21} = 0.142$, $\tau_{21} = 140MPa$, $p_{hyd} = 600MPa$.
$\{\overline{R}\} = (1378, 950, 40, 125, 97)^T MPa$, $\{E\} = (129000, 129000, 5600, 5600, 1330)^T MPa$,
$m = 2.8$, $v_{\perp//} = 0.32$, $b_{\perp//} = 0.12$, $v_{23} = 0.48$, $G_{23} = 1860MPa$, $E_{m0} = 950MPa$, $v_m = 0.35$,
$\{\varepsilon_{fr}\} = (1.07, 0.74, 0.43, 2.8, 8.6)^T \%$. $2^{nd}Tg$ shift effect not considered. Part A curve: $b_{\perp//} = 0.3$

Fig. TC 3. Failure shear strain $\gamma_{21}(\sigma_2 = -p_{hyd})$ in dependence of an increasing p_{hyd}. UD T300 carbon/PR319 epoxy hoop wound tube. Properties, see TC2. Two 0° test data (circles) are shown for information and Annex 5 calculation. Part A curve: $b_{\perp//} = 0.3$ (dashed)

Fig. TC 4. Shear stress- shear strain curves for $\tau_{21}(\gamma_{21})$ for $\sigma_{hyd} = 0$, -600 MPa. UD T300 carbon/PR319 epoxy hoop wound tube. Properties, see TC2 and section 4.2. $\tau_{21} \equiv \tau_{out}$. Part A curve: $b_{\perp//} = 0.3$ (dotted)

Fig. TC 5. Tri-axial failure state of stress: σ_2 vs. longitudinal stress $\sigma_1(=\sigma_3)$ for a UD E-glass/MY750epoxy cube.
$\{\overline{R}\} = (1280, 800, 40, 145, 73)^T MPa$, $\{\varepsilon_{fr}\} = (2.81, 1.75, 0.25, 1.2, 4)^T \%$, $v_{\perp//} = 0.28$. $b_{\perp\perp} = 1.16$,
$v_m = 0.35$, $E_{m0} = 3350MPa$, $G_{m0} = E_{m0}/(2 + 2 \cdot v_m)$, $m = 2.8$, $b_{\perp\|} = 0.2$. Data from fit:
$\{a\} = (-, -, -0.3, -2.17, -8.0)$, $\{b\} = (-, -, 0.013, 0.21, 0.87)^T$,
$\{E\} = (-, -, 16200, 16200, 5188)^T MPa$, $\{n\} = (-, -, 8.5, 7.0, 8.8)^T$. Part A: $b_{\perp\perp} = 1.21$

Fig. TC 6. Through-thickness stress $\sigma_3(=\sigma_2)$ vs. fibre-parallel stress σ_1, UD S2-glass/epoxy waisted test specimen. $\{\overline{R}\} = (1700, 1150, 63, 180, 72)^T MPa$, $v_{\perp//} = 0.3$, $m = 2.8$, $b_{\perp\perp} = 1.21$,
$b_{\perp//} = 0.12$, $\{\varepsilon_{fr}\} = (2.81, -1.75, 0.25, -1.2, 4)^T \%$, $\{E\} = (-, -, 16200, 16200, 5188)^T MPa$,
$E_{m0} = 3350MPa$, $v_m = 0.35$, $G_{m0} = E_{m0}/(2 + 2 \cdot v_m)$. From data fit: $\{n\} = (-, -, 8.5, 7.0, 8.8)^T$,
$\{a_s\} = (-, -, -0.3, -2.17, -8.0)$, $\{b_s\} = (-, -, 0.013, 0.21, 0.87)^T$, $\{\overline{R}_{p0.2}\} = (-, -, 156, 137, 54.6)^T MPa$

Fig. TC 7. Through-thickness stress $\sigma_3(=\sigma_2)$ vs. fibre-parallel stress σ_1. UD A-S carbon/epoxy1.

$\{\overline{R}\}=(1990,\ 1500,\ 38,\ 150,\ 70)^T\ MPa$, $\nu_{\perp//}=0.3$, $\{E\}=(140,\ 140,\ 10,\ 10,\ 6)^T\ GPa$

Fig. TC 8. Effect of the applied surface pressure $\sigma_z=-p$ (through-thickness stress) on the size of the normal section force $n_y=\hat{\sigma}_y/t$ at fracture when $n_x/t=\hat{\sigma}_x=\sigma_z$.

Thick-walled tube, UD lamina-composed laminate [35/-35/35/-35], E-glass/MY750/epoxy. Properties and stress states, see TC5. Computation path for TC9 is indicated

Fig. TC 9.

Comparison between theoretical predicted stress-strain curves $\hat{\sigma}_y(\hat{\varepsilon}_x)$ and $\hat{\sigma}_y(\hat{\varepsilon}_y)$ and experimental data for a [35/-35/35/-35]s E-glass/MY750 epoxy laminate. Continuous curves are the predicted curves; measured data (+), taken from [Kad09]. Properties and loading, see TC8 Monotonically loaded $\hat{\sigma}_x=\hat{\sigma}_y=\sigma_z$ up to -100 MPa, then $\hat{\sigma}_y=n_y/t$ grows further

Fig. TC 10. Applied section shear load-caused maximum-thickness failure shear stress τ_{zy} vs. applied through-thickness stress σ_z for a [45/0/-45/90]$_{ns}$, carbon/epoxy laminate, IM7/8551-7.

$\sigma_x=\sigma_y=0$, $E_{m0}=4080MPa$, $\nu_{\perp\parallel}=0.34$. $G_{m0}=E_{m0}/(2+2\cdot\nu_m)$, $\nu_m=0.38$, $E_\parallel=165000MPa$, $E_\perp=8400MPa$, $G_{\parallel\perp}=5600\ MPa$; $R_z^t=63MPa$. $\{\overline{R}\}=(2560,\ 1590,\ 73,\ 185,\ 90)^T\ MPa$, $\{e_{fr}\}=(1.55,\ 1.1,\ 0.87,\ 3.2,\ 5)^T\%$; assumed: $b_{\perp\perp}=1.2$, $b_{\perp\parallel}=0.2$, $\hat{\sigma}_z^{cr,TC10}=-1000MPa$, $m=2.5$ (safe side). Provided test data: + , x

Fig. TC 11. Thickness failure shear stress τ_{zy} vs. applied through-thickness stress $\sigma_z=-p$ for a [0/90/0/90]$_{ns}$. Properties, see TC10; $\hat{\sigma}_z^{cr,TC11}=-1100MPa$ (assumed). Lower curve is basic model

Fig. TC 12. Predicted single stress-strain curve caused by a through-thickness compressive stress $\sigma_z=-p$ for a [0/90/0/90]$_{ns}$ versus test data (+) from a quasi-isotropic laminate [45/0/-45/90]$_{ns}$, $\sigma_x=\sigma_y=0$. Curves: (a) Part A, $E_\perp=8400MPa$; (b) Part B, $E_\perp=11000MPa$; (c) Part B, $E_\perp=11000MPa$ with Eq.(11). Properties, see TC10; $\sigma_z^{max}=-1400MPa$, $m=2.5$

Table 1. Main features of the FMC and the non-linear analysis

04.04.2014